Corona Gold Ltd

Garfield Copper–Gold Project

Historical Geophysical Data Review

by K. Blundell

SGC Report No. 2186

May 2011

CLIENT	Corona Gold Ltd
Project Name	Garfield
COUNTRY	Australia
PROVINCE	Tasmania
1:250,000 SHEET	Queenstown (SK-5505)
1:100,000 SHEET	Franklin (8013)
Method Keywords	IP, Magnetics
Commodity	Cu, Au

SOUTHERN GEOSCIENCE CONSULTANTS

TABLE OF CONTENTS

APPENDICES

LIST OF FIGURES

LIST OF TABLES

SUMMARY

Garfield is a base-metals prospect, located within the Mount Read Volcanics in the Queenstown area of western Tasmania. The geology of the Garfield prospect is dominated by early Palaeozoic volcanics, which host numerous styles of mineralisation. The focus of exploration within the Garfield prospect is intrusion-related Cu-Au mineralisation (Prince Lyell/West Lyell type) associated with a mapped andesite intrusion through the centre of the prospect. RGC Exploration Pty Ltd acquired ground magnetic data and two phases of gradient array and dipole-dipole IP data as part of their exploration program over the Garfied Prospect between 1993 and 1995. These data have been reprocessed, modelled and interpreted by SGC as part of a review by the project's new owners, Corona Gold Ltd.

Grids of the ground magnetic data confirm that the mapped andesite units have variable magnetic properties. Those either side of the main southwest-northeast fault (F1) are moderately magnetic, but similar mapped units to the north are not.

3D modelling performed on the located magnetic data shows consistent moderate westerly dips for the magnetic units in the centre of the survey grid, and confirms that the historic drilling orientation in this area was appropriate for targeting potential mineralisation associated with these magnetic units. However, the existing drilling has only tested the margins of the magnetic models, and therefore the Cu/Au intersections in GAR001 and GAR002 may not be representative of the main part of the mineralised system. An additional drill hole is recommended to test the centre of the magnetic model.

The geometry of the model for the magnetic body to the south of F1 is very different from the models to the north, and appears to be a depth-limited slap-like body. NCT008 may have tested the northern limit of the magnetic source, but an alternative model suggests that the source has not yet been tested by drilling to date.

Dipole-dipole Line 1800N, acquired to follow-up a gradient array anomaly in the southwestern part of the area, show a strongly chargeable source at the south western end of the line, well west of the gradient array anomaly. A 2D inversion model of the DDIP data show a chargeability high at about 50m depth and coincident local resistivity low. The regional magnetics show no significant magnetic anomaly at this location. The model lies on the margin of mapped volcanicalstics, and could therefore represent a possible VHMS target. Further dipole-dipole and gradient array surveying is recommended to better define the anomaly and constrain its extents.

The gradient array data generally show good chargeability anomalies coincident with the magnetic anomalies and mapped andesite units, and therefore magnetite may represent the chargeable source for these gradient IP anomalies. However, there are numerous gradient array anomalies to the north, also coincident with the mapped andesite units, which do not have any significant magnetic response. These gradient IP anomalies are confirmed by 2D inversion models of two dipole-dipole IP lines, 2800N and 3000N. Of the 10 models identified from the 2D inversion for these lines, five are within or near mapped andesite intrusives and/or dacite lavas and volcanicalstics, and are therefore considered interesting targets. Further dipole-dipole surveying is recommended to better define these models and test the correlation of models between lines. The other 2D IP models appear to be surficial sources within unfavourable lithologies.

1.0 INTRODUCTION

Garfield is a base-metals prospect, located within the Mount Read Volcanics in the Queenstown area of western Tasmania. The focus of exploration within the Garfield prospect is intrusion-related Cu-Au mineralisation (Prince Lyell/West Lyell type) associated with a mapped andesite intrusion through the centre of the prospect.

The ground has previously been explored by BHP Billiton, RGC Pty Ltd and Newcrest. RGC Exploration Pty Ltd has conducted the majority of geophysical surveys over the area, and acquired ground magnetic data and two phases of gradient array and dipole-dipole IP data as part of their exploration program over the Garfied Prospect between 1993 and 1995. These data have been reprocessed, modelled and interpreted by SGC as part of a review by the project's new owners, Corona Gold Ltd.

This report documents the results of a comprehensive review of historical geophysical datasets over the Garfield Prospect, with the aim of confirming previous models and interpretations, providing alternative models where appropriate, and identifying any new targets of interest.

The data reviewed in this report includes ground magnetics, and two phases of gradient array and dipole-dipole IP acquired for RGC Exploration Pty Ltd. Some limited DHTEM surveying was carried out on five holes in the area, but these logs are barren of any anomalies and so are not discussed further in this report.

All coordinates presented in this report utilise the GDA94 Datum and MGA55 grid projection.

2.0 GEOPHYSICAL DATASETS

Datasets included for review include a single phase of ground magnetic data, two phases of gradient array IP data, and three lines of Dipole-Dipole IP data (Table 1).

Table 1. Supplied geophysical survey data files

Supplied Data File	Description	Coordinate System	Date	Source	Contractor
td1800.dat (rgc1800.dat)	Dipole-Dipole IP data for line1800N	Local	Dec 1993	RGC	Geoterrex
td2200.dat	Raw Gradient array data (incomplete - lies 1800, 1900, 2000 only)	Local	Dec 1993	RGC	Geoterrex
td2200.xyz	Binned gradient array data	Local	Dec 1993	RGC	Geoterrex
gradient.xyz	Processed gradient array data (all channels and binned data)	Local	Dec 1993	RGC	Geoterrex
iprgc805.dat	Raw Gradient array data	Local	Dec 1993	RGC	Geoterrex
iprgc805.xyz	Geosoft xyz format processed IP (no headers)	Local	Dec 1993	RGC	Geoterrex
gad2800n.dat	Dipole-Dipole IP data for line2800N	Local	Dec 1995	RGC	Quadrant Geophysics
gad3000n.dat	Dipole-Dipole IP data for line3000N	Local	Dec 1995	RGC	Quadrant Geophysics
gargrid.dat	Processed gradient array data	Local	Oct 1995	RGC	Quadrant Geophysics
279,298,317,318a, 318b.mob	Un-located round magnetic field data	-	Dec 1993	RGC	
297,298,317,318. mon	Base station data	-	Dec 1993	RGC	
garmag.readme	Relation between field data reading number, time code and local coordinates	Local	Dec 1993	RGC	
link.dat	Control points (100m intervals) relating local coordinates with AMG55 coordinates for groundmag traverses (incomplete)	Local/AMG55	Dec 1993	RGC	
all.red	Incomplete located and corrected groundmag data file	Local	Dec 1993	RGC	

3.0 Local Grid Transform and Possible Coordinate Errors

No details of the conversion used between AGD66/AMG55 and the local grid were provided in the supplied data compilation. The two sources that can be used to determine the relationship between local and AMG55 coordinates are a file called "link.dat" included with the December 1993 ground magnetic data, and a plan (drawing ID 5532/185) from the April 1994 – March 1995 annual report. The "link.dat" file contains control points that relate the magnetic local grid positions back to AGD66/AMG55 every 100m along 14 survey lines, some (but not all) of which are annotated on the plan 5532/185. However, the local ground magnetic grid is not regular, and therefore the transformation to AGD66/AMG55 coordinates varies depending on which set of control points are selected. This is further complicated by the local grid depicted on the plan, which shows duplicate lines from different vintages for 2200N, 2400N, 2600N and 2800N which are spatially separated by up to 75m in the local northing.

Given the lack of a definitive local transform, the best compromise was attained by best fitting a rectangular grid outline to the extents of the magnetic grid for which coordinate pairs were supplied in the "link.dat" file (Figure 1).

Figure 1 shows the relationship between the derived local grid outline (red) and grid points (red circles), ground magnetic survey control points (blue crosses) and the combined local grid lines. A good fit was obtained between the local grid outline and all of the outer control points from the ground magnetic survey, with a maximum deviation from the grid outline of 5m. In addition, the locations of most of the ground magnetic survey control points for lines 3000N, 2000N, 1800N, 1800E, 2000E, and 2100E fit well with the derived local grid points. Note that actual control points documented in the "link.dat" file were used to locate the ground magnetic data.

The dipole-dipole IP lines are on 1800N, 2800N, and 3000N; the transformed MGA55 positions of dipoles for this survey are consistent whether the December 1993 ground magnetic control points or the SGC derived local grid transform are used. Thus, the confidence in the MGA55 location of the electrodes is considered high, and the electrodes are likely to be within 5–10m of their true position.

The December 1993 gradient array survey lines are assumed to have been surveyed along the same lines as the ground magnetics, and therefore utilise the same control points. There are no control points for lines 2900 and 3100 from the October 1995 gradient array data, so the SGC derived local grid transform was used to locate these lines.

Table 2 details the final control points used for transforming coordinates in this review between GDA94/MGA55 and the local grid at Garfield. The rotation of the local grid with respect to true north is 052.8°. It is recommended that any future ground work in the area utilise this local grid so as to easily combine old and new datasets.

Table 2. Derived Local Grid Control Points

Control Point	***Local East***	***Local North***	***MGA55 Easting 3***	***MGA55 Northing***
1	1500	1600	379986.72	5324135.87
2	1500	3200	379019.37	5325410.32
3	2600	3200	379895.55	5326075.37
4	2600	1600	380862.91	5324800.92

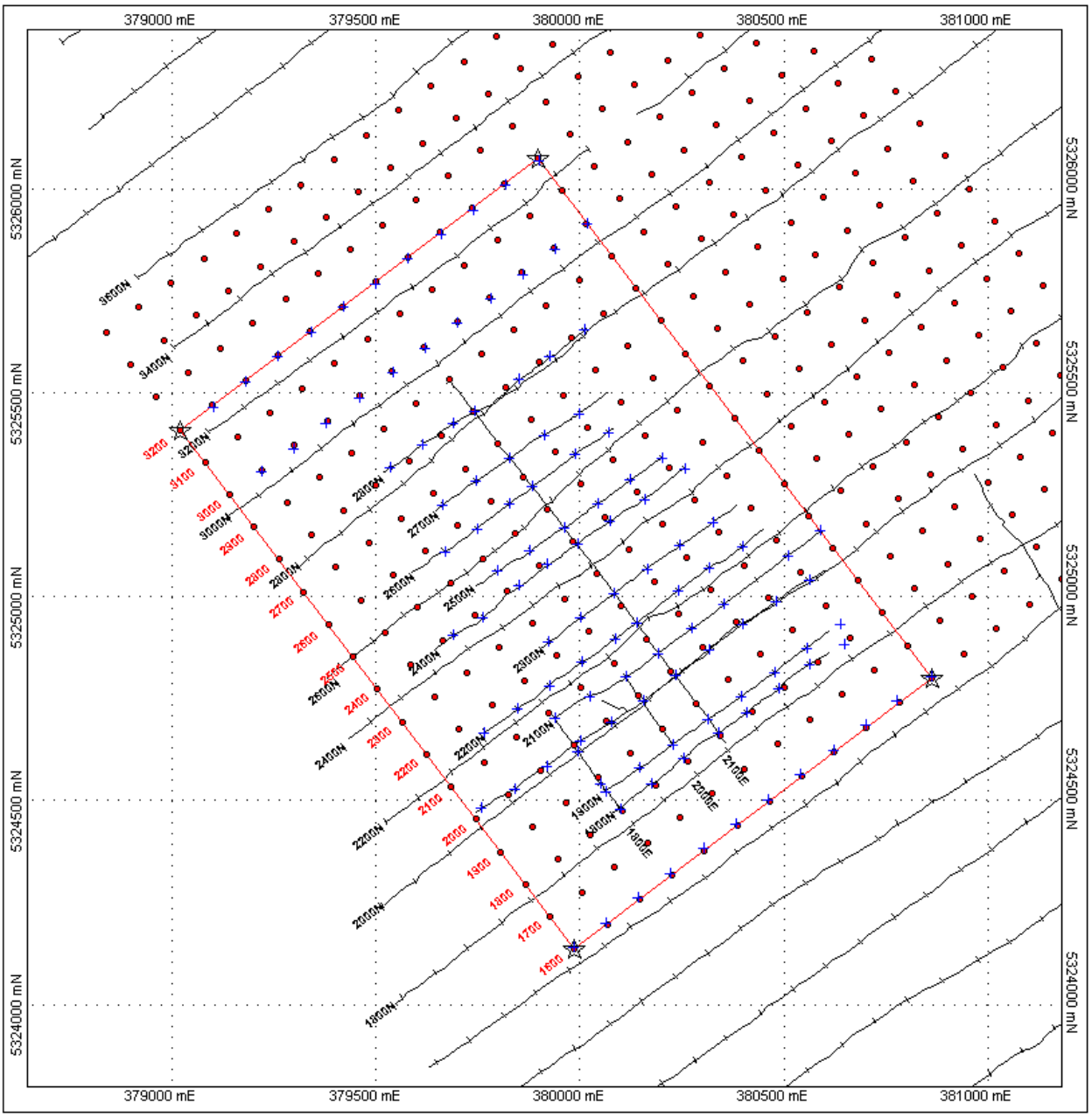

Figure 1: Relationship between old local grid, RGC local grid and the best fit SGC derived local grid (red circles). The latter was derived by the best fit to the ground magnetic survey control points (blue crosses)

4.0 DATA PROCESSING

4.1. Ground magnetic data

Detailed ground magnetic surveying took place during November and December 1993 (Mudge 1994). No metadata were supplied in the RGC Report of supplied data files, but the report indicates that the data were processed in-house by RGC. The supplied data include raw field and base station files, various control files, and a final processed data file. Analysis of the latter shows that, although the entire dataset must have been processed at some stage by RGC (Figure 2), this file represents an incomplete dataset, which is critically missing most of line 2200N over the main magnetic anomaly (Figure 3). Therefore, SGC undertook to reprocess the raw data to obtain a full processed dataset and in doing so, provide an independent check that the original processing was done correctly. The final processed magnetics in shown in Figure 4.

The processing revealed multiple acquisition and documentation errors, which significantly increased the time taken to accomplish what should be a relatively straight forward job. In addition, the supplied control points did not cover the extents of the survey. Additional "dummy" control points were derived by extending the trend of the control points and assuming a constant 5m station interval.

The following steps were undertaken to process the raw data.

1. Create base station database — apply non-linear filter to remove spikes, remove average baseline, and interpolate readings at 5 second intervals
2. Create field-data database — use look up table to apply base station correction
3. Create time/location control database — interpolate to 5m between control points.
4. Use lookup table to assign local coordinates to field-data database.
5. Create local grid/MGA55 control database — interpolate to 5m between control points.
6. Use lookup table to assign MGA55 coordinates to field-data database.
7. Compare overlapping and repeated data, and remove noisier readings.
8. Apply elevation values to reading locations (for 2D modelling).

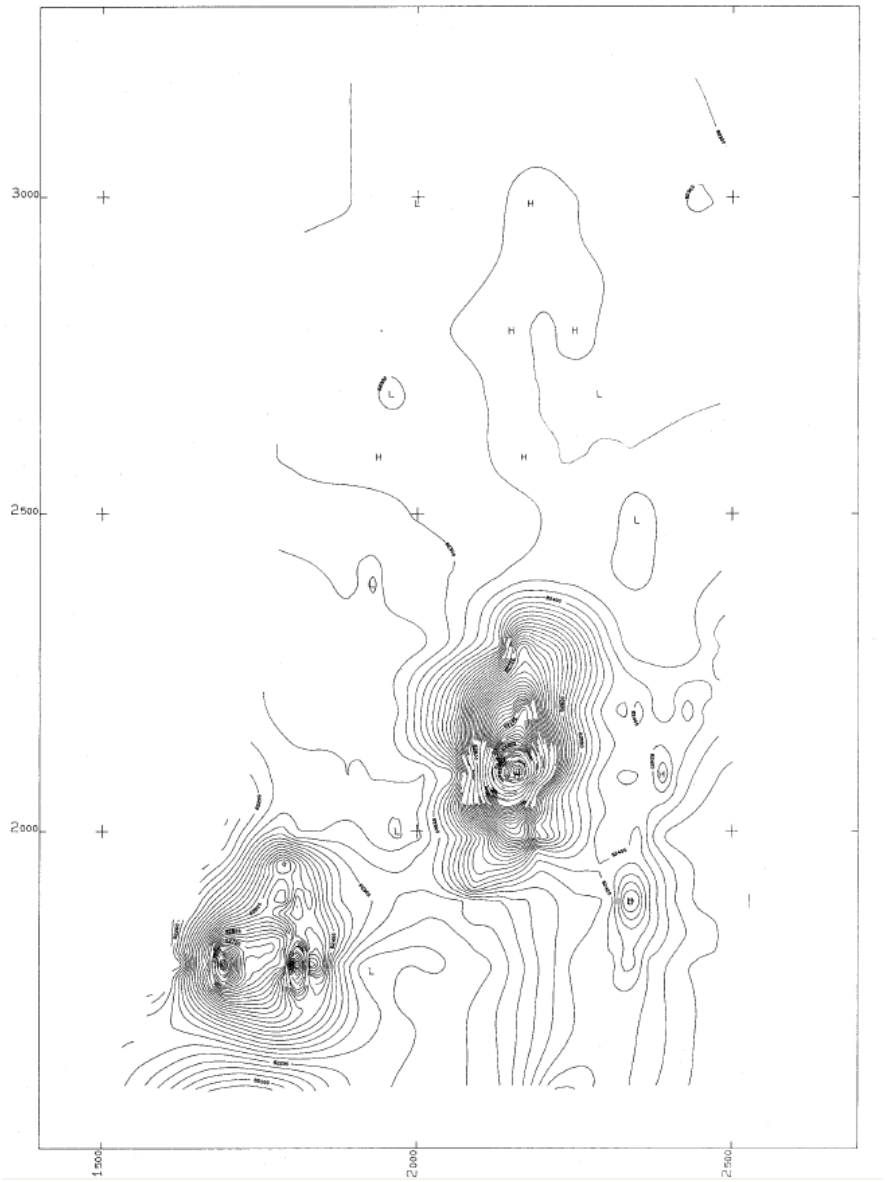

Figure 2: Extract from Mudge (1994) showing the TMI contours for the full ground magnetic survey (in local coordinates)

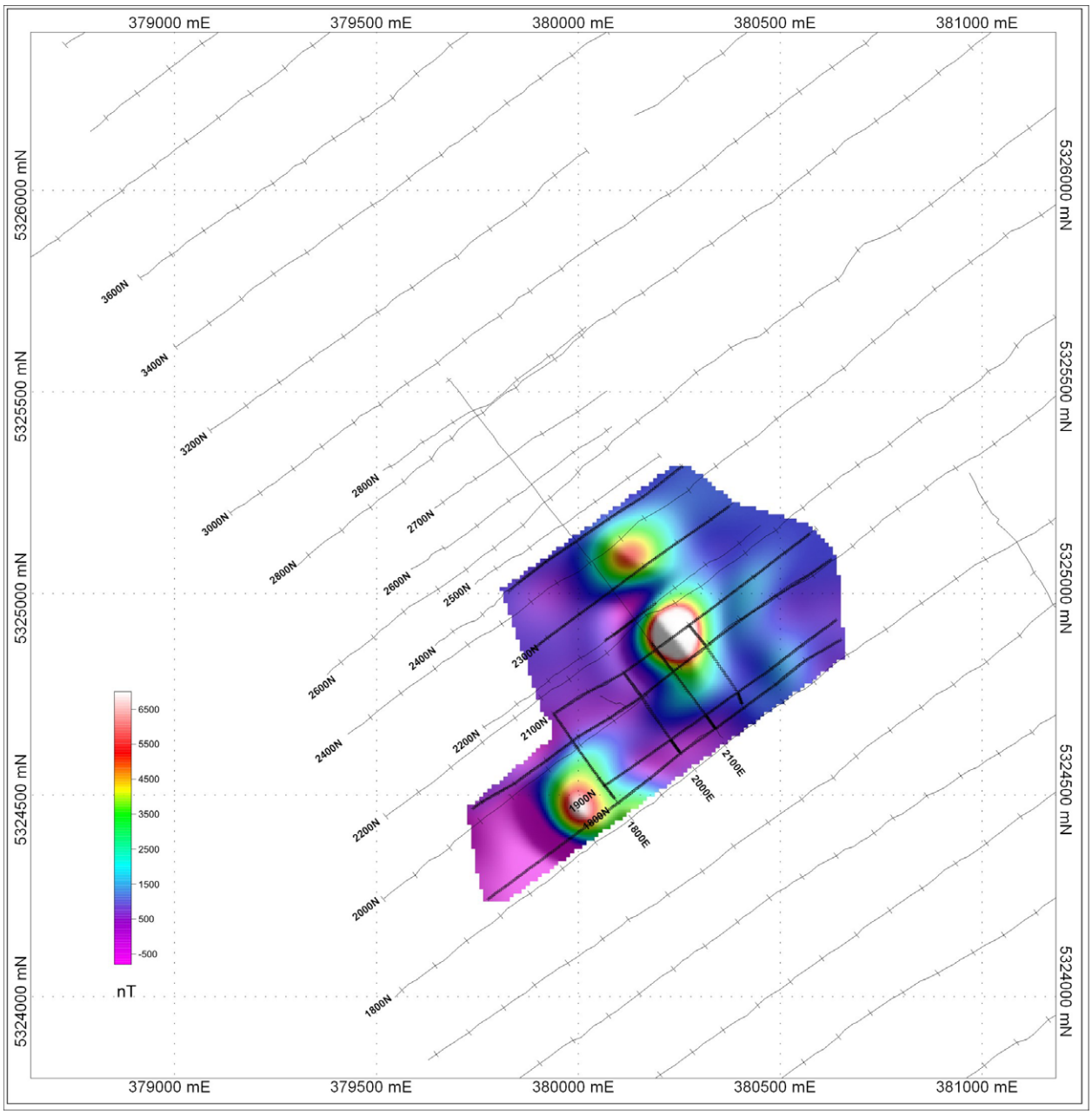

Figure 3: Extents and TMI grid of the supplied processed ground magnetic data. Bold lines represent supplied data points

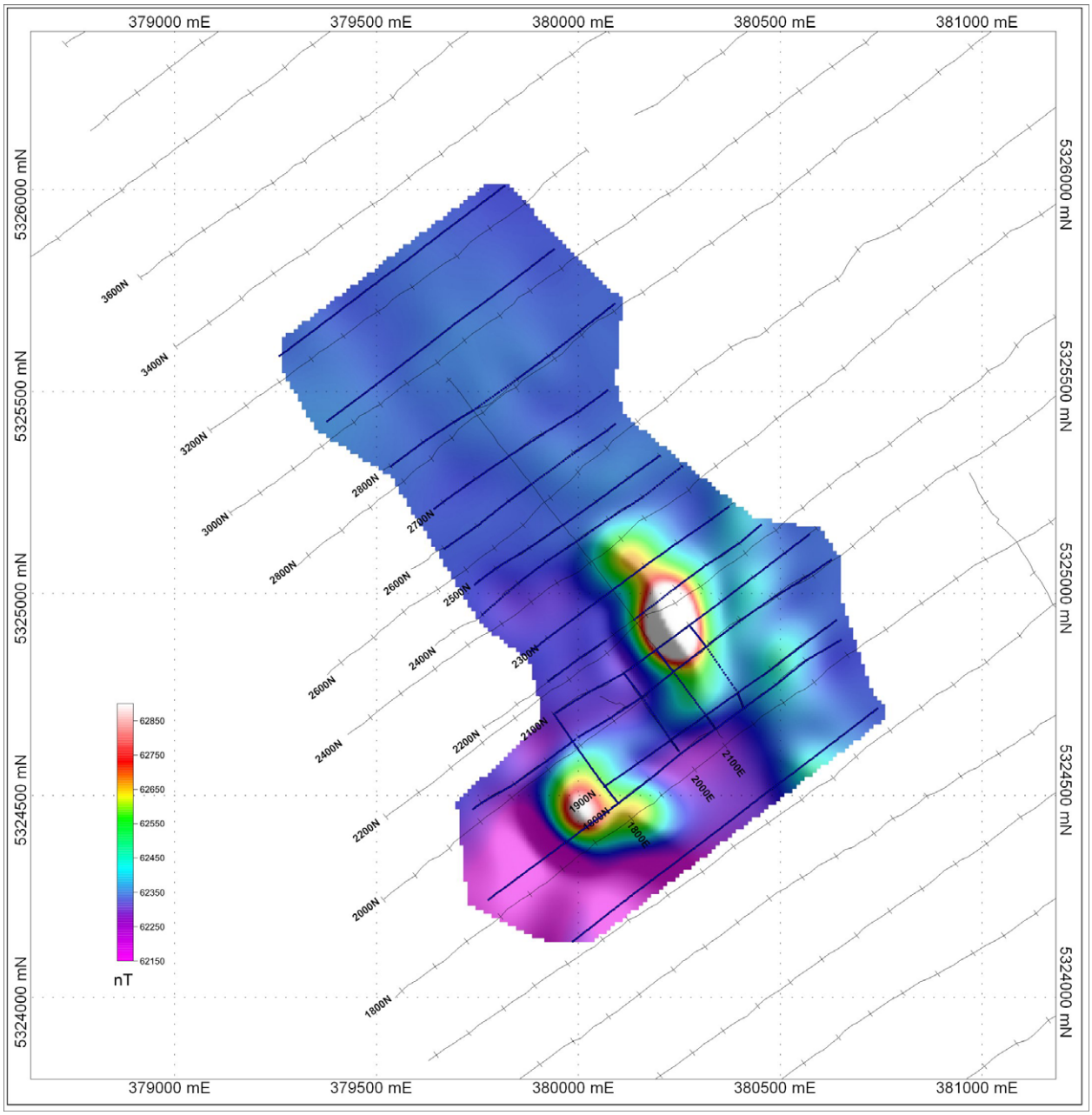

Figure 4: Extents of the supplied un-processed ground magnetic data, and TMI grid of the final SGC processed data. Bold lines represent supplied data points

The final SGC reprocessed ground magnetic grid (Figure 3) is consistent with the original contours from (Figure 2). However, the grid derived from the incomplete RGC processed datasets (Figure 3) is misleading, in that the main magnetic anomaly between 2000N and 2400N appears as two discrete magnetic highs. Therefore, despite the time taken, it was considered worthwhile effort to reprocess the data in full in order to obtain a digital version of the entire ground magnetic survey.

4.2. Gradient Array IP/Resistivity Data

There were two phases of gradient array surveying in the area: Geoterrex acquired eight lines of data during December 1993, and Quandrant Geophysics acquired an additional five lines of data during September–October 1995.

4.2.1. Geoterrex 1993

The coverage of the Geoterrex 1993 gradient array survey data are outlined in Table 3.

Survey Details:

Receiver: Zonge GDP-16
Transmitter: Huntec 7.5kW
Frequency: 0.5 Hz (2-second pulse)
Rx Dipole Spacing: 50m
Reading Interval: 25m
Tx Dipole Spacing: 1800m

No control points for transforming between local grid coordinates and AMG55. It was assumed that the gradient array IP lines were coincident with the ground magnetic traverses, and therefore the ground magnetic control points were used to locate the data relative to the MGA55 grid system (Figures 5 and 6).

There were several supplied data files. A combination of "td2200.xyz" and "gradient.xyz" were used, as together these provided a full datasets of un-binned channel data, and processed IP and Resistivity values.

Table 3. Geoterrex 1993 Gradient Array survey Coverage

Line	***Stn From***	***Stn To***
1800	1600	2500
1900	1800	2475
2000	1700	2500
2100	1800	2500
2200	1700	2500
2300	1900	2475
2400	1800	2400
2600	1800	2500

4.2.2. Quadrant 1995

The coverage of the Quadrant Geophysics gradient array survey data are outlined in Table 4.

Survey Details:

Receiver: Scintrex IPR-12
Transmitter: Zonge GGT-2.5 2.5kW
Frequency: 0.5 Hz (2-second pulse)
Rx Dipole Spacing: 50m
Reading Interval: 25m
Tx Dipole Spacing: 1800m

Only one data file was supplied "gargrid.dat" — this file only contains processed data (Mx binned between 540 and 1100msec).

No control points for transforming between local grid coordinates and AMG55. It was assumed that the gradient array IP lines would be on a local grid consistent with the ground magnetic traverses and gradient array survey from 1995. The 1993 magnetic control points for lines 2800N, 3000N and 3200N were used to directly locate the associated data from the 1995 gradient IP survey, and the derived local grid transform (see Section 1) was used to locate the intermediate lines 2900N and 3100N, relative to the MGA55 grid system (Figures 5 and 6).

Table 4. Quadrant Geophysics 1995 Gradient Array survey Coverage

Line	***Stn From***	***Stn To***
2800	1825	2475
2900	1825	2550
3000	1825	2600
3100	1825	2575
3200	1825	2600

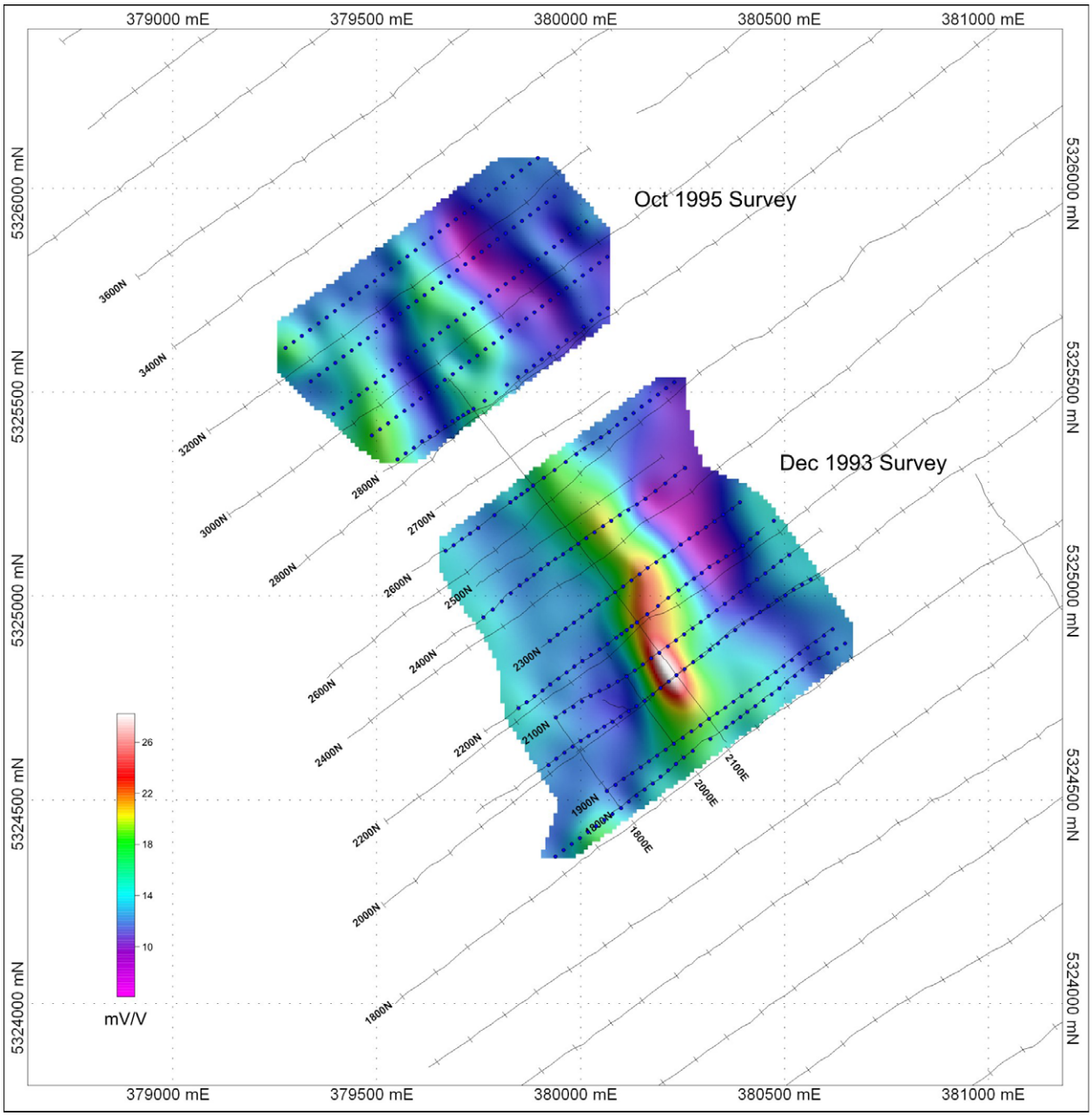

Figure 5: Image of apparent chargeability for the two phases of gradient array surveying. Blue dots represent the assumed reading locations for these datasets.

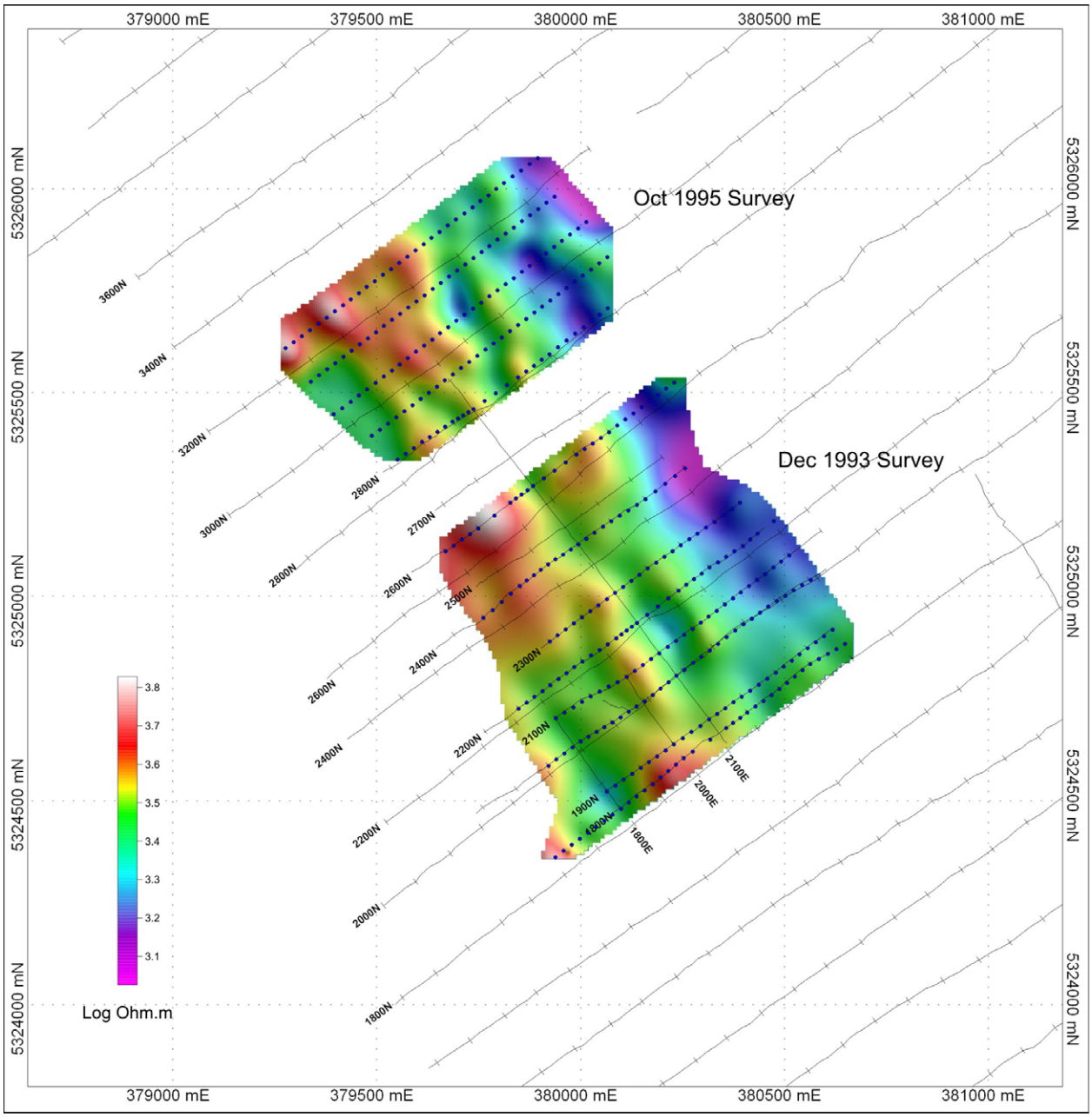

Figure 6: Image of apparent resistivity for the two phases of gradient array surveying. Blue dots represent the assumed reading locations for these datasets.

4.3. Dipole-Dipole IP/Resistivity Data

Along with the gradient array data, there were two phases of Dipole-Dipole data acquired in the: Geoterrex a single line to complement the December 1993 gradient array data, and Quandrant Geophysics acquired two lines to the north to complement the September–October 1995 gradient array data (Figure 7).

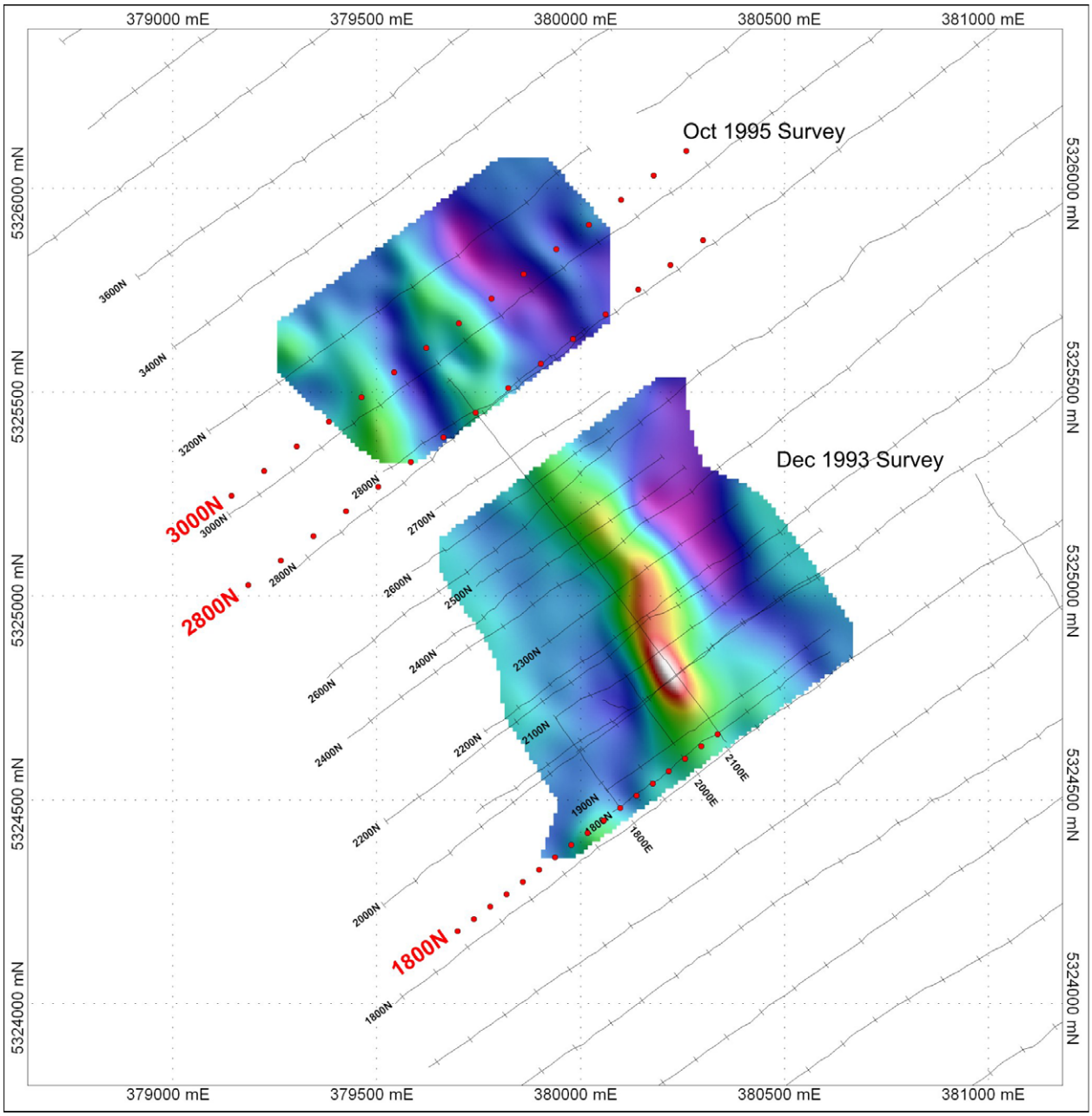

Figure 7: Locations of the three D-D IP lines surveyed, relative to the gradient array surveys. Red dots represent the assumed electrode positions

4.3.1. Geoterrex 1993

Survey Details:

Lines Surveyed:	1800N
Receiver:	Zonge GDP-16
Transmitter:	Huntec 7.5kW
Frequency:	0.5 Hz (2-second pulse)
Rx Dipole Spacing:	50m
Reading Interval:	50m
Tx Dipole Spacing:	50m

Only one data file was supplied this line "rgc1800.dat". Again, no control points for transforming between local grid coordinates and AMG55, so the control points from the 1993 magnetic survey for line 1800N was used to directly locate the associated data relative to the MGA55 grid system (Figure 7).

The data were imported to SGC's in-house IP processing software for QC and cleaning. Analysis of the data confirmed that all the readings were low-noise and useable (Figure 8).

Calculated apparent resistivity and chargeability sections (Figure 9) show no obvious bad data points in the data. Elevations were added to the electrode locations for more-accurate inversion of the data

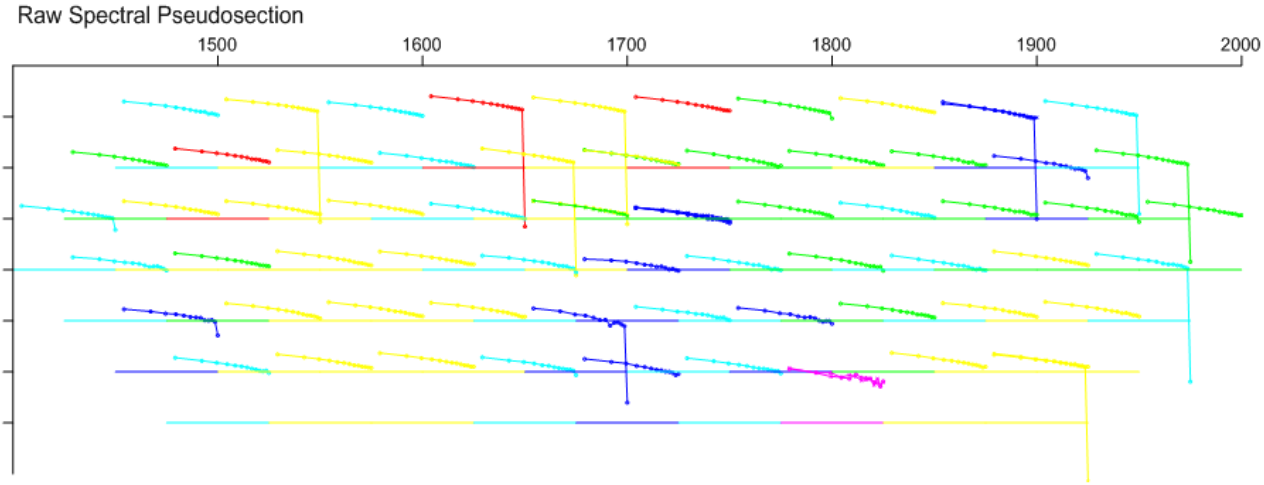

Figure 8: Raw spectral pseudosection for line 1800N showing clean IP decays for all readings

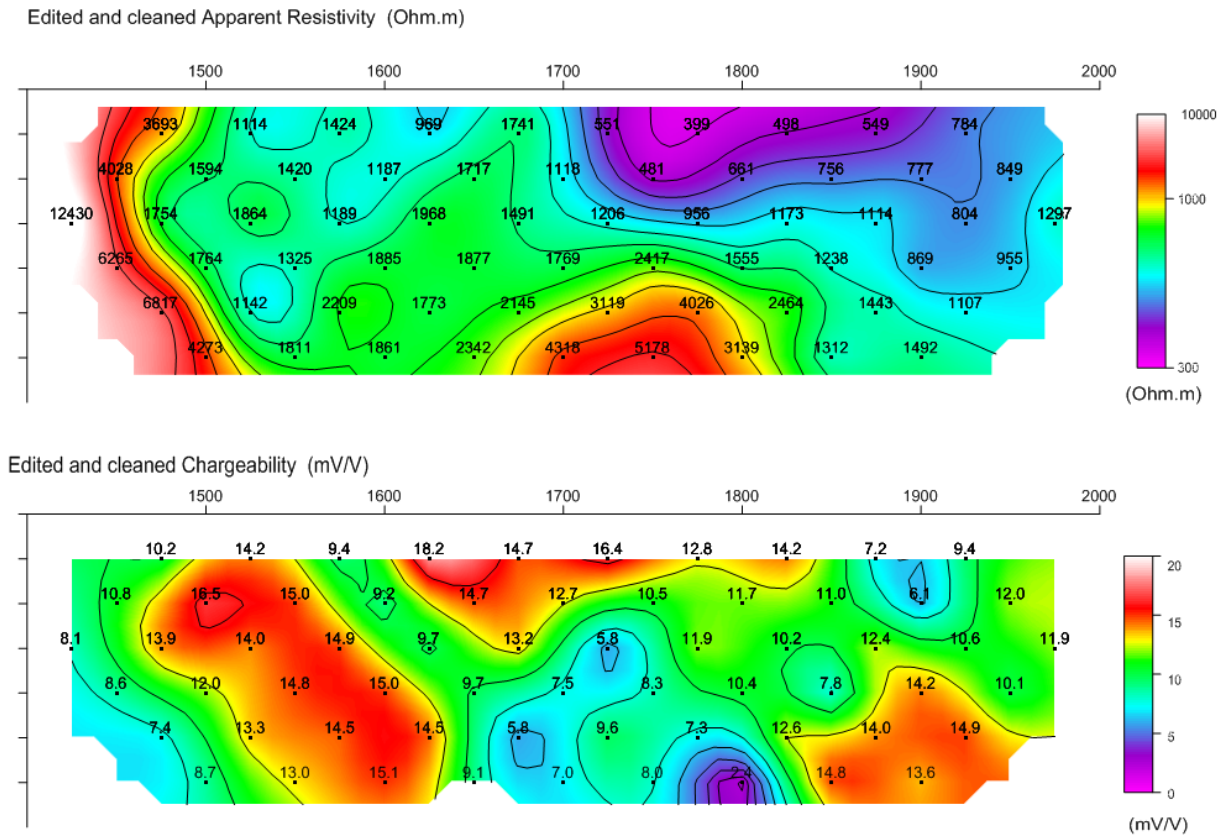

Figure 9: Apparent resistivity and chargeability sections for line 1800N

4.3.2. Quadrant 1995

The coverage of the Quadrant Geophysics gradient array survey data are outlined in Table 3.

Survey Details:

Lines Surveyed:	2800N & 3000N
Receiver:	Scintrex IPR-12
Transmitter:	Zonge GGT-2.5 2.5kW
Frequency:	0.5 Hz (2-second pulse)
Rx Dipole Spacing:	100m
Reading Interval:	100m
Tx Dipole Spacing:	100m

Only one data file was supplied for each line "gad2800n.dat" and "gad3000n.dat". Again, no control points for transforming between local grid coordinates and AMG55, so the control points from the 1993 magnetic survey for lines 2800N and 3000N were used to directly locate the associated data relative to the MGA55 grid system (Figure 7).

The data were imported to SGC's in-house IP processing software for QC and cleaning. Analysis of the data for line 2800N showed two problem data points: a flipped decay and evidence for EM coupling — these readings were removed before further processing (Figure 10). Similarly, there were several bad readings caused by EM coupling for the 3000N data that were removed prior to producing calculated apparent resistivity and chargeability sections and modelling the data (Figure 11).

Calculated apparent resistivity and chargeability sections of the edited data for these lines (Figures 12 and 13) show no obvious erroneous values. Elevations were added to the electrode locations for more-accurate inversion of the data

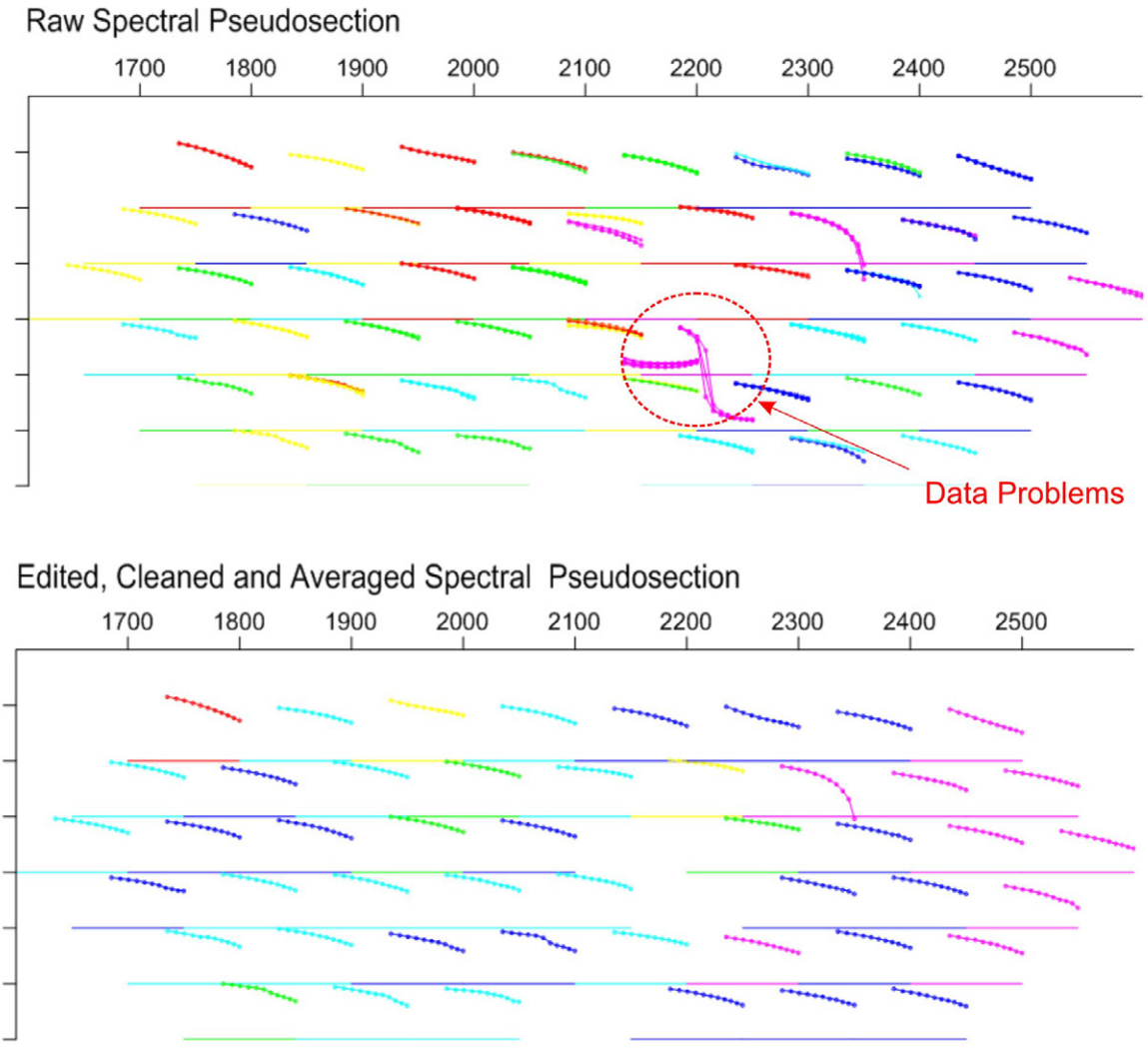

Figure 10: Raw spectral pseudosection for Line 2800N showing problem decays

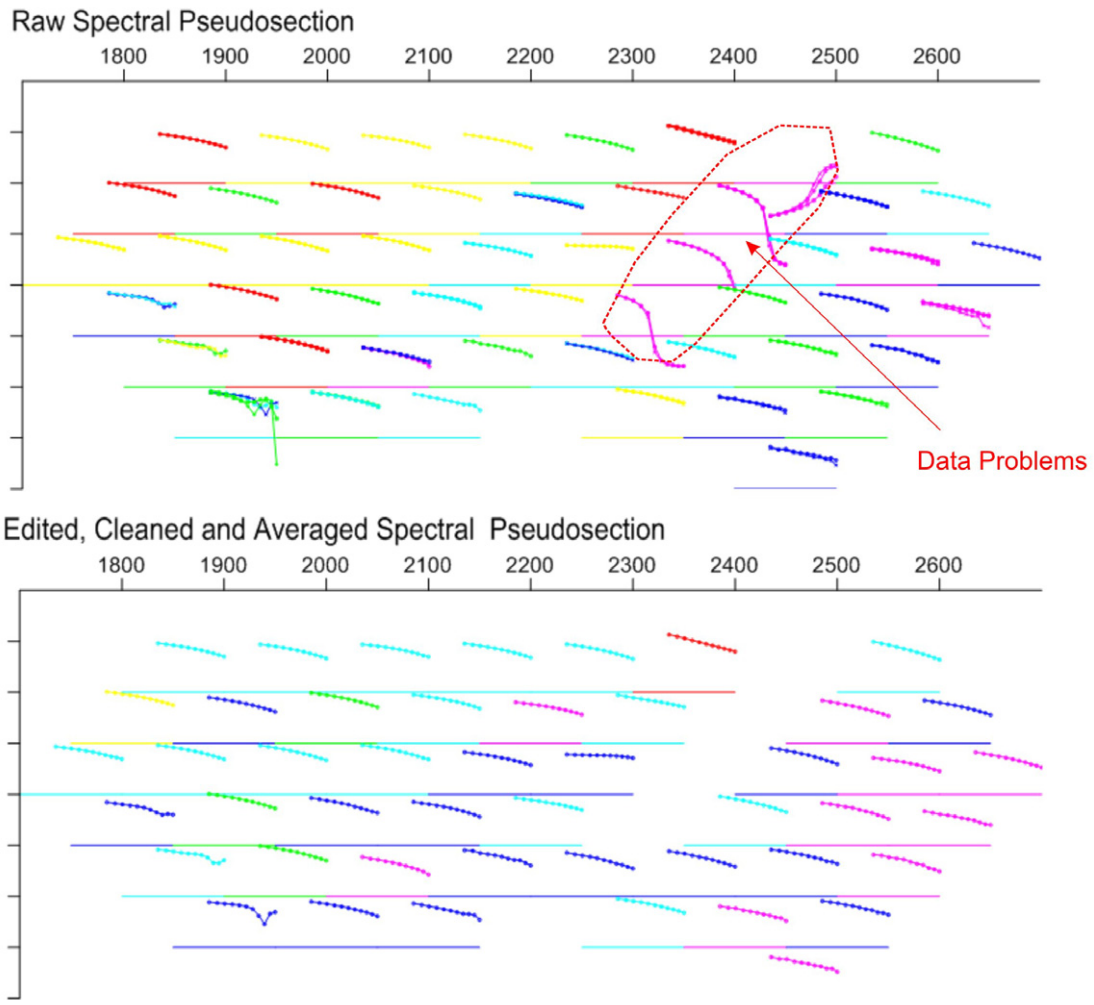

Figure 11: Raw spectral pseudosection for Line 3000N showing problem decays

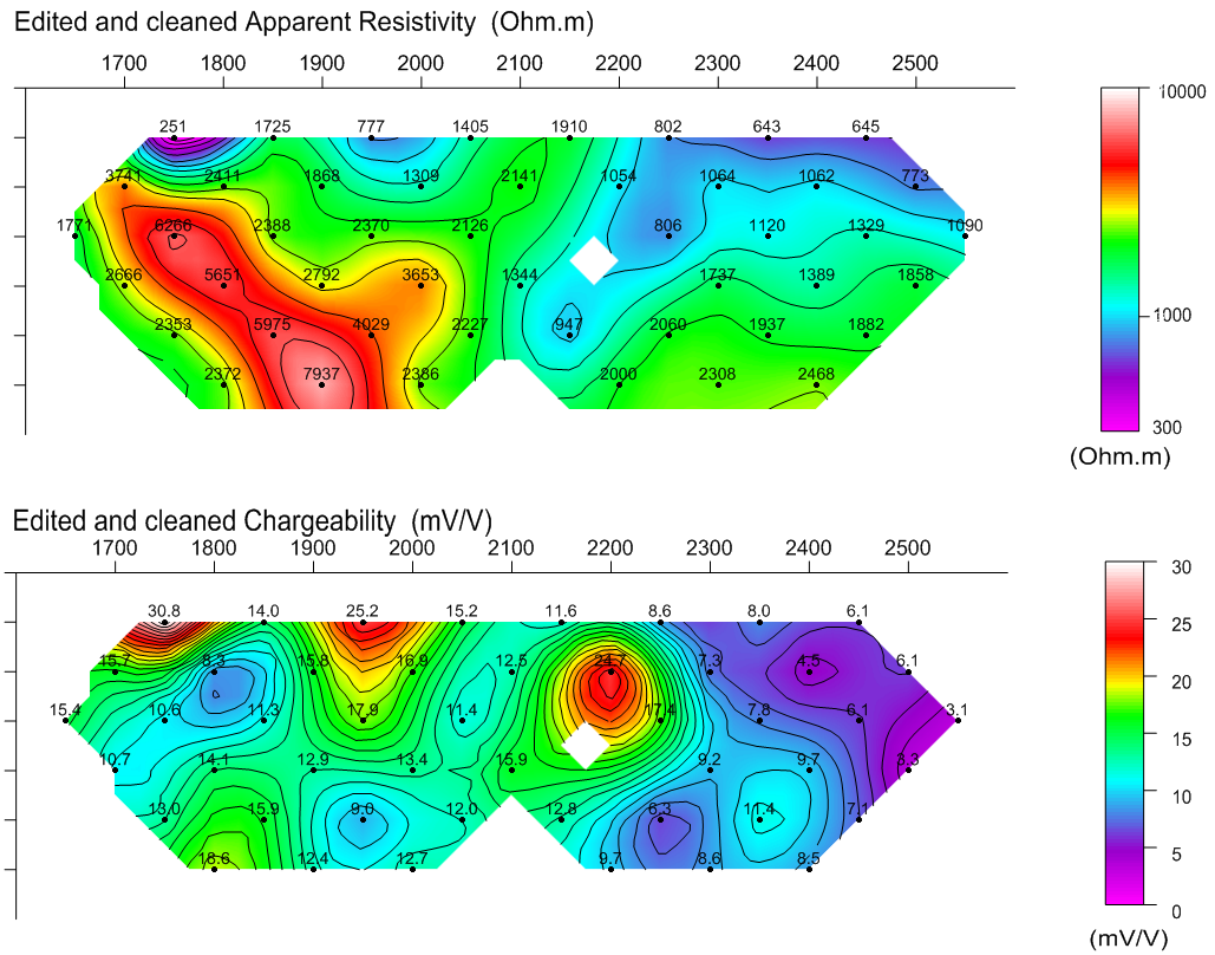

Figure 12: Apparent resistivity and chargeability sections for line 2800N

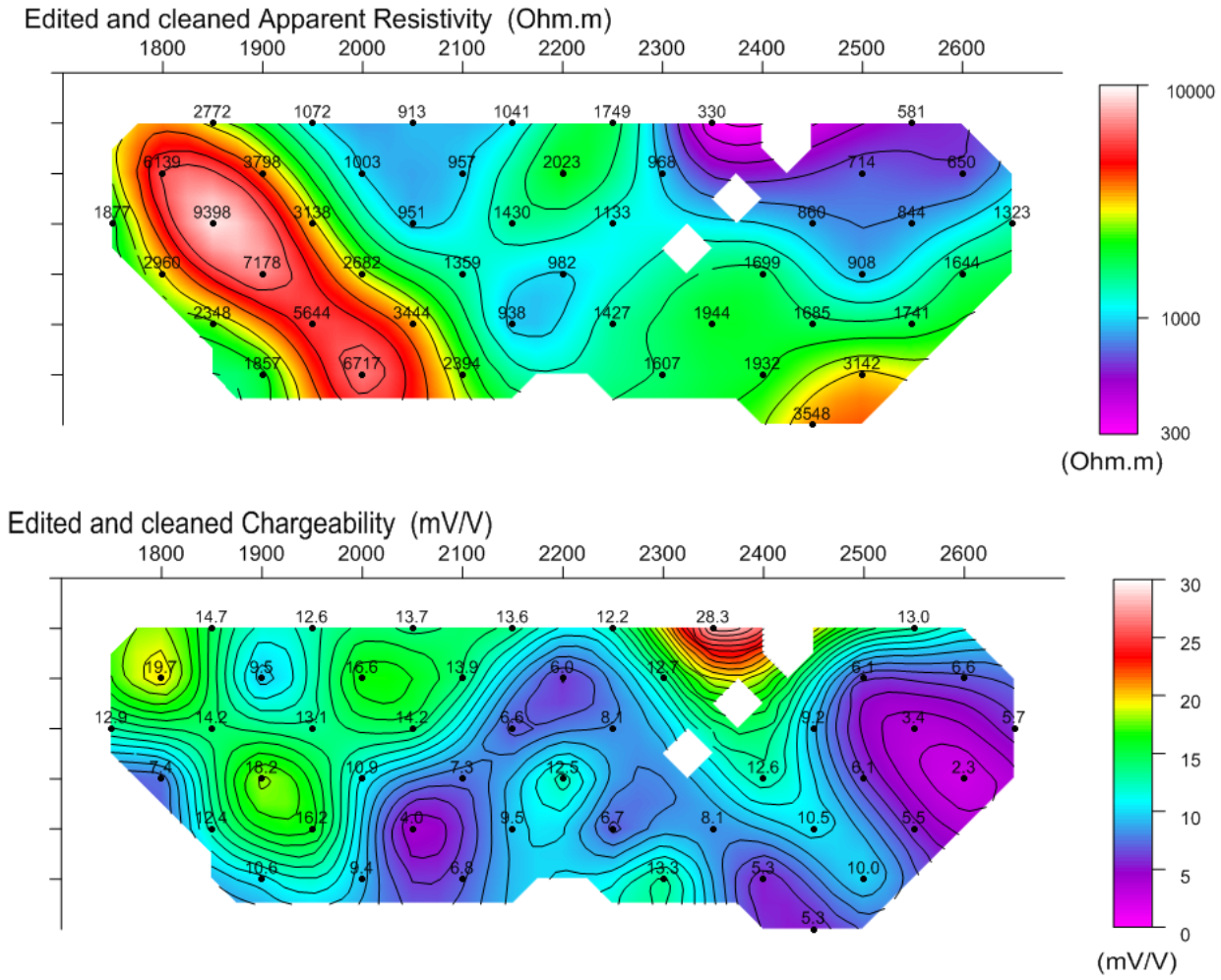

Figure 13: Apparent resistivity and chargeability sections for line 3000N

5.0 MODELLING, INVERSION AND INTERPRETATION

5.1 Gradient Array Data

Figure 14 shows the SGC processed gradient array chargeability data and the interpreted gradient array anomalies and faults from Mudge (1994) and Roberts (1995). The locations of the anomalies from Mudge (1994) are interpreted form the text, as Plan 8 (Interpretation Plan) from this report was missing. The SGC image below confirms the four anomalies described by Mudge (1994), although IP2 and IP3 are considered to represent the same source. Mudge (1994) discusses apparent dips based on asymmetry of the gradient array IP data, and suggests that the source of IP1 is dipping to the east, whereas the source of IP2 is dipping to the west. The asymmetry for the central part of the IP1-IP2 trend is certainly consistent with a westerly dip, but the asymmetry for the main part of the anomaly IP1 is not as clear, and may just represent a lateral variation in background chargeability.

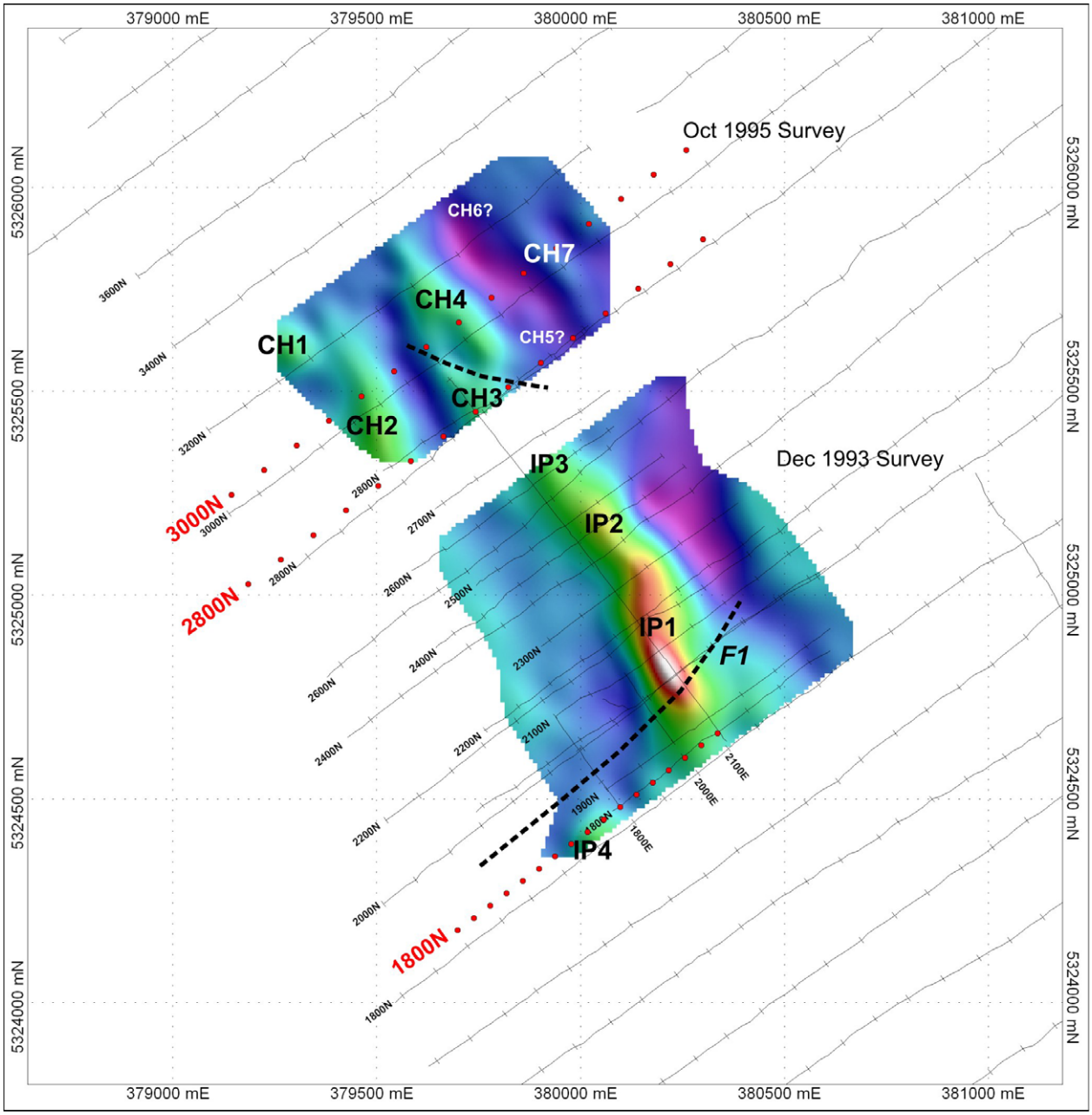

Figure 14: Interpreted gradient array anomalies from Mudge (1994) and Roberts (1995)

Roberts (1995) identified seven discrete gradient array IP anomalies, although CH5 and CH6 are not confirmed by the SGC processing. If real, these are very subtle anomalies and not considered to be significant.

Figure 15 shows the interpreted solid geology for the area. The strong gradient IP anomaly IP1 is coincident with a strong magnetic anomaly and mapped andesite. Rocks containing relatively high concentrations of magnetite can in some cases be relatively chargeable, and therefore the magnetic andesite intrusion here is a possible source for the IP anomaly. Mapped andesite to the south of F1 also has coincident magnetic anomaly and gradient array IP (IP4) anomalies. However, the andesite units mapped to the north of IP1 have corresponding gradient array IP anomalies (IP2/3 and CH3-4) but no corresponding magnetic anomaly — this suggests that magnetite is not the source of these IP anomalies. Anomalies CH1 and CH2 are located within bedded siltstone (shales?) and sandstone, the former which can also be good IP sources if pyritic and graphitic in nature. CH2 is coincident with low resistivity, which may also indicate a conductive shale unit.

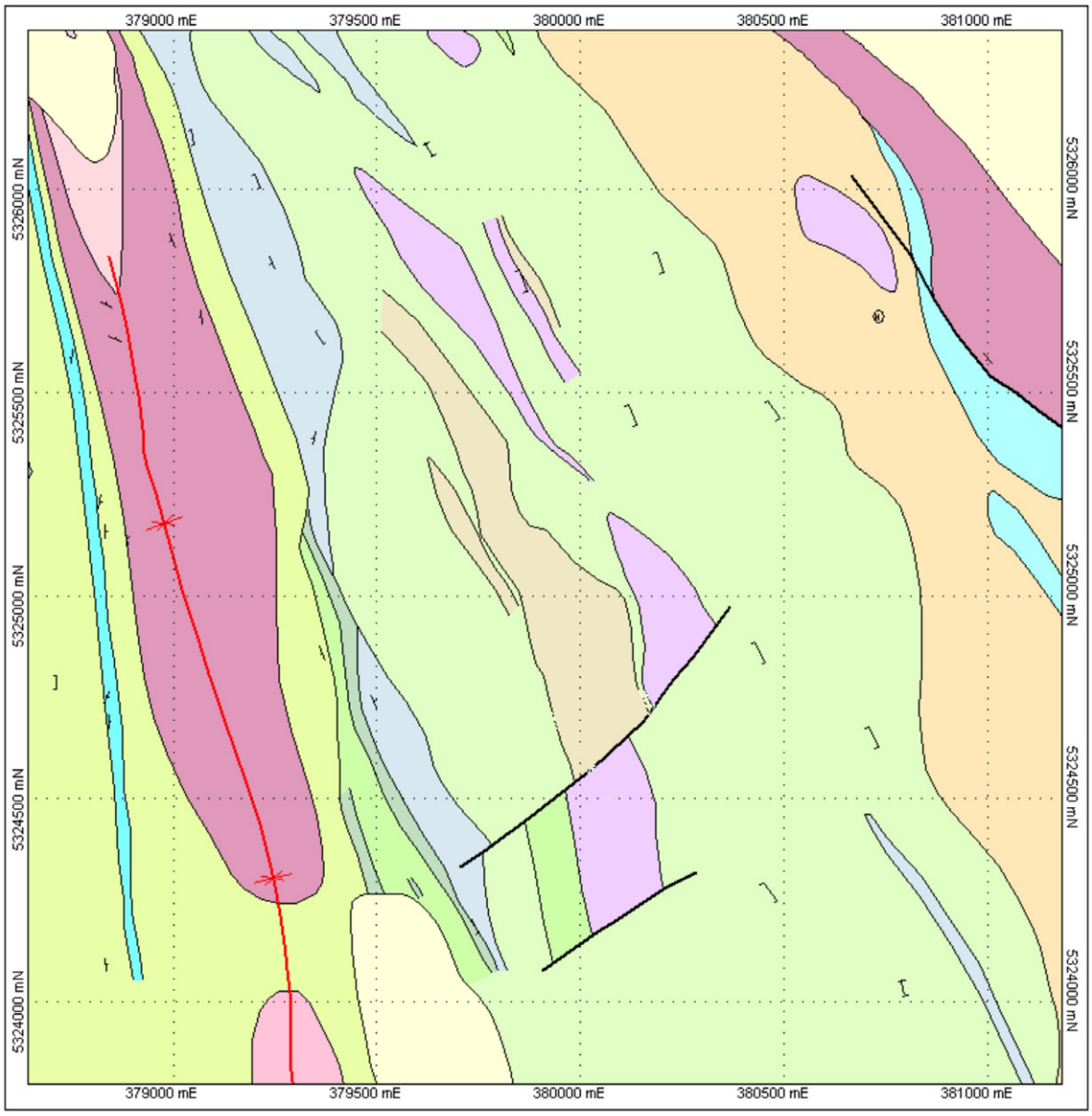

Figure 15: Interpreted solid geology (as supplied by Corona Gold)

5.2 Dipole-Dipole IP Inversions

2D inversions were carried out on the three lines of Dipole-Dipole IP/resistivity data using Loke Res2DInv software. The inversion parameters used are documented in Appendix 2.

The inversion results were compared with the observed apparent resistivity and chargeability data to data to ensure the resulting inversion model was reasonable representation of the observed data.

Figures 17 to 18 show the inversion results for Lines 1800N, 2800N, and 3000N respectively. In these figures, the black points represent the extents of the inversion mesh, but the models have been trimmed on sensitivity (20% cut off) and to the original survey extents to remove parts of the models that are considered unreliable.

5.2.1 Line 1800

Line 1800N was acquired in order to follow-up gradient array anomaly IP4. Mudge (1994) does not present any modelling for this data for which to compare to the SGC inversion. The raw IP data and IP inversion model for line 1800 show a strongly chargeable source (1A on Figure 16) at the south western end of the line at about 1500E, well west of the location of IP4, which is at around 1700E. Model 1A is further supported by a local resistivity low at this location, making this an attractive target. There is no gradient array data covering this area, but the ground magnetic grid does extend to this area, and shows no magnetic source. The model sits at the western margin of a volcaniclastic unit, so may be of interest in terms of possible VHMS-style mineralisation.

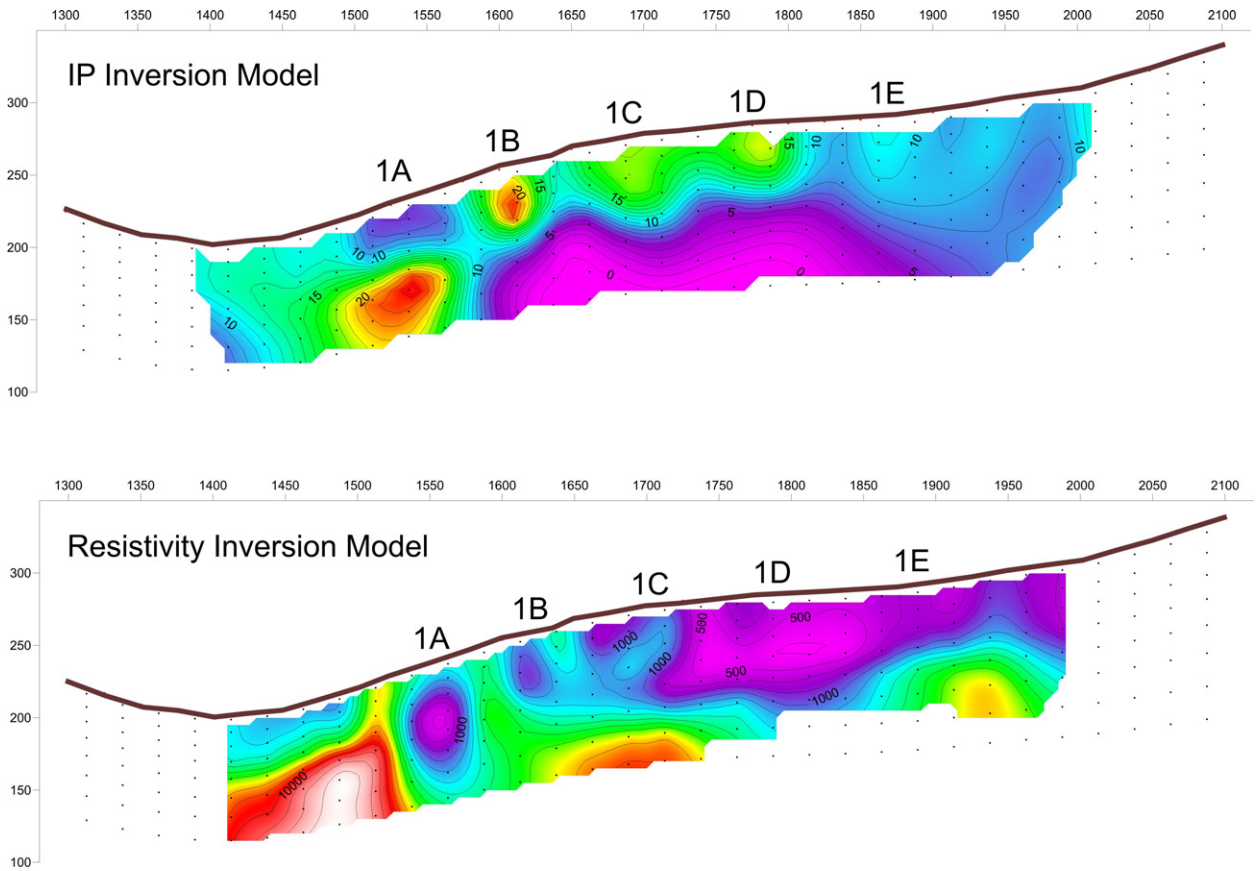

Figure 16: 2D Inversion model for line 1800

Model 1B, at about 1600E, is also an interesting local IP high/resistivity low with no magnetic response, and sits at the eastern margin of the volcaniclastic unit.

Model 1C/1D is coincident with gradient array anomaly IP4 and the local ground magnetic anomaly in this area and is attributed to the andesitic intrusion.

Model 1E is a broad subtle chargeable feature that, if real, may be an offline response of the main part of the andesite intrusion to the north. Alternatively, there is a subtle broad gradient array anomaly extending south from IP1 over this area, so model 1E may represent a local lateral variation in the background chargeability.

None of these models have been tested by drilling — GAR004 is the closest drill hole, but was drilled under model 1C.

5.2.2 Line 2800

The inversion models for Line 2800N (Figure 17) correlate very well with the gradient data and are somewhat consistent with the models derived in Roberts (1995). The shallow IP models 2A/2B are coincident with gradient array anomaly CH2, model 2C corresponds CH3, and model 2D corresponds with the subtle anomaly CH5. The resistivity model for this line does not show a lot of lateral variation, which is at odds with the inversion model for line 3000N.

Models 2C and 2D are considered the most interesting features from this line. 2C is coincident with the mapped dacitic lavas and volcaniclastics and may be related to model 3C from line 3000N (see below). Model 2D is in the vicinity of andesite–mafic units. Both have no associated magnetic anomaly, which discounts magnetite as a potential source.

Model 2A/2B are low priority — they look to be regolith related, and are not sited within prospective geology.

None of these anomalies has been tested with drilling to date.

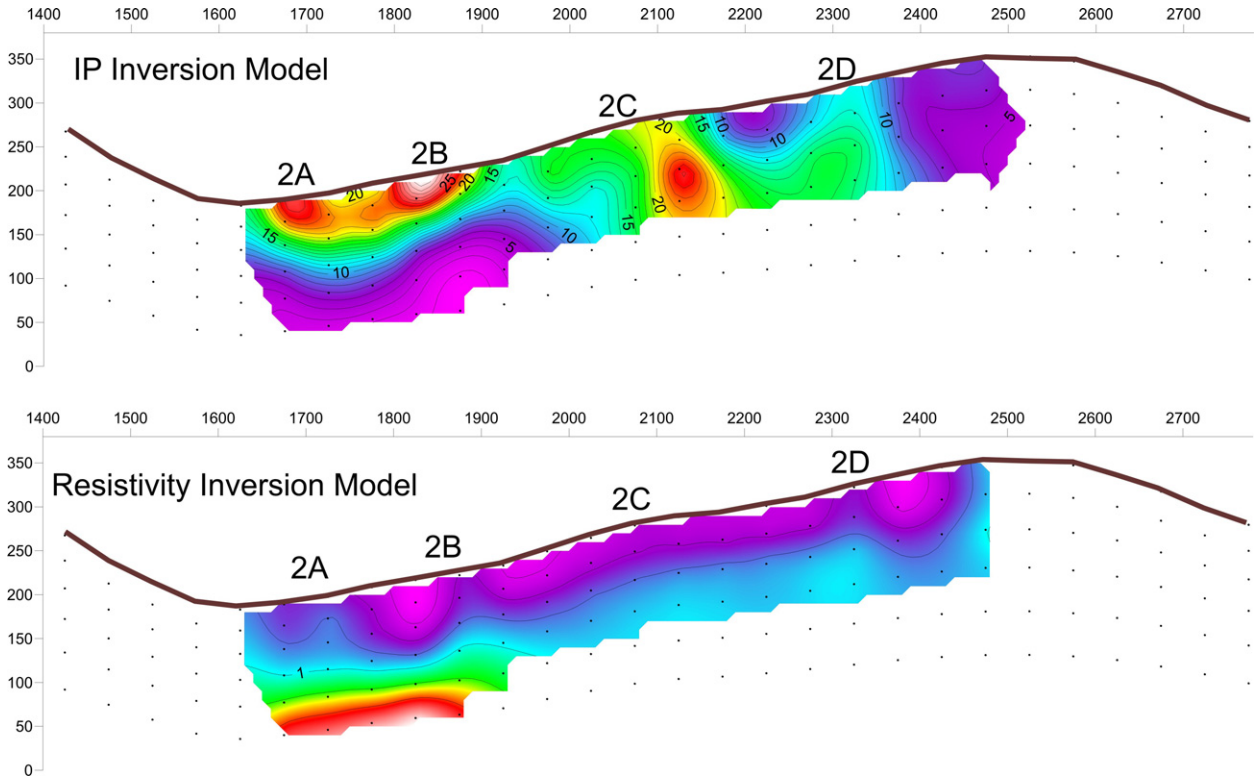

Figure 17: 2D Inversion model for line 2800

5.2.3 Line 3000

The inversion models for Line 3000N (Figure 18) also correlate very well with the gradient data. IP model 3B is coincident with gradient array anomaly CH2, model 3C corresponds CH4, model 3D corresponds with the subtle anomaly CH5, and model 3E corresponds with CH7. Models 3A and 3F on the edge of the line extend past the gradient array grid, so cannot be confirmed. All of these IP models, with the exception of 3A, are associated with resistivity lows. Again, there are no magnetic anomalies of note to suggest the IP anomalies are from magnetite-rich sources.

Model 3C is the most interesting feature on this line. It lies on the western margin of the mapped andesite, between this and dacitic lavas and volcaniclastics, and may extend to depth (3G). As discussed above, it may extend to model 2C on line 2800N, but the gradient data shows some structural complexity between these lines (Figure 14), so these models may not be directly related. The model in Roberts (1995) included a chargeable bodies corresponding to 3A, 3C, 3E and 3F, but did not have a discrete model for 3B or 3D. The former is within a sequence of siltstone and sandstone, and may be associated with graphitic/pyritic sediments. Models 3D and 3E correlate well with mapped andesite units.

None of these anomalies have been tested with drilling to date.

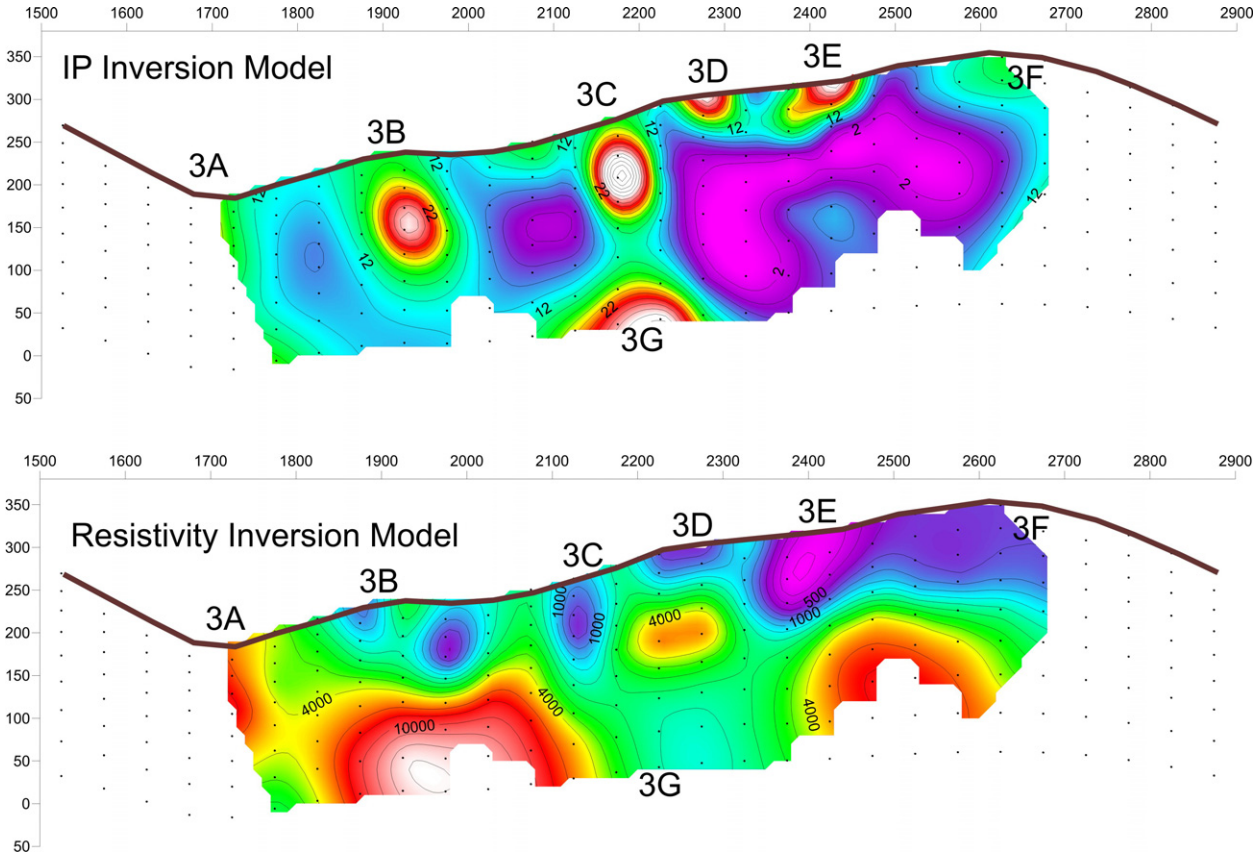

Figure 18: 2D Inversion model for line 3000

5.3 Magnetic modelling

Some simple 3D magnetic modelling was carried out over the magnetic anomalies along four traverses between 1800N and 2300N (Figure 19) to confirm the dip of the models presented in Mudge (1994). The naming convention has been kept consistent, with model A representing the source of the magnetic high in the southwestern part of the grid between 1700N and 1900N, model B representing the main andesite intrusion between 2000N and 2200N, and model C representing an extension of the andesite to the north to about 2400N. Some of the models in Mudge (1994) were complicated shapes, and the previous modelling did not take into account the topography. Thus the SGC revised models incorporate the topography and aim at trying to get consistent model fits using simple dipping dyke-like models of limited strike length. The modelling from Mudge (1994) took into account some remanance information from tests done on samples from GAR001 (Schmidt, 1993). However, Schmidt (1993) recognised that the main remnant vector was roughly parallel to strike and therefore contributes little to the anomaly. He also found than both remanence and susceptibility decrease with depth. Therefore, no remanence was incorporated into the revised modelled carried out here.

Figure 19 shows the plan view of the models and model lines with respect to the gridded ground magnetic data. A summary of the main model parameters are presented in Table 4.

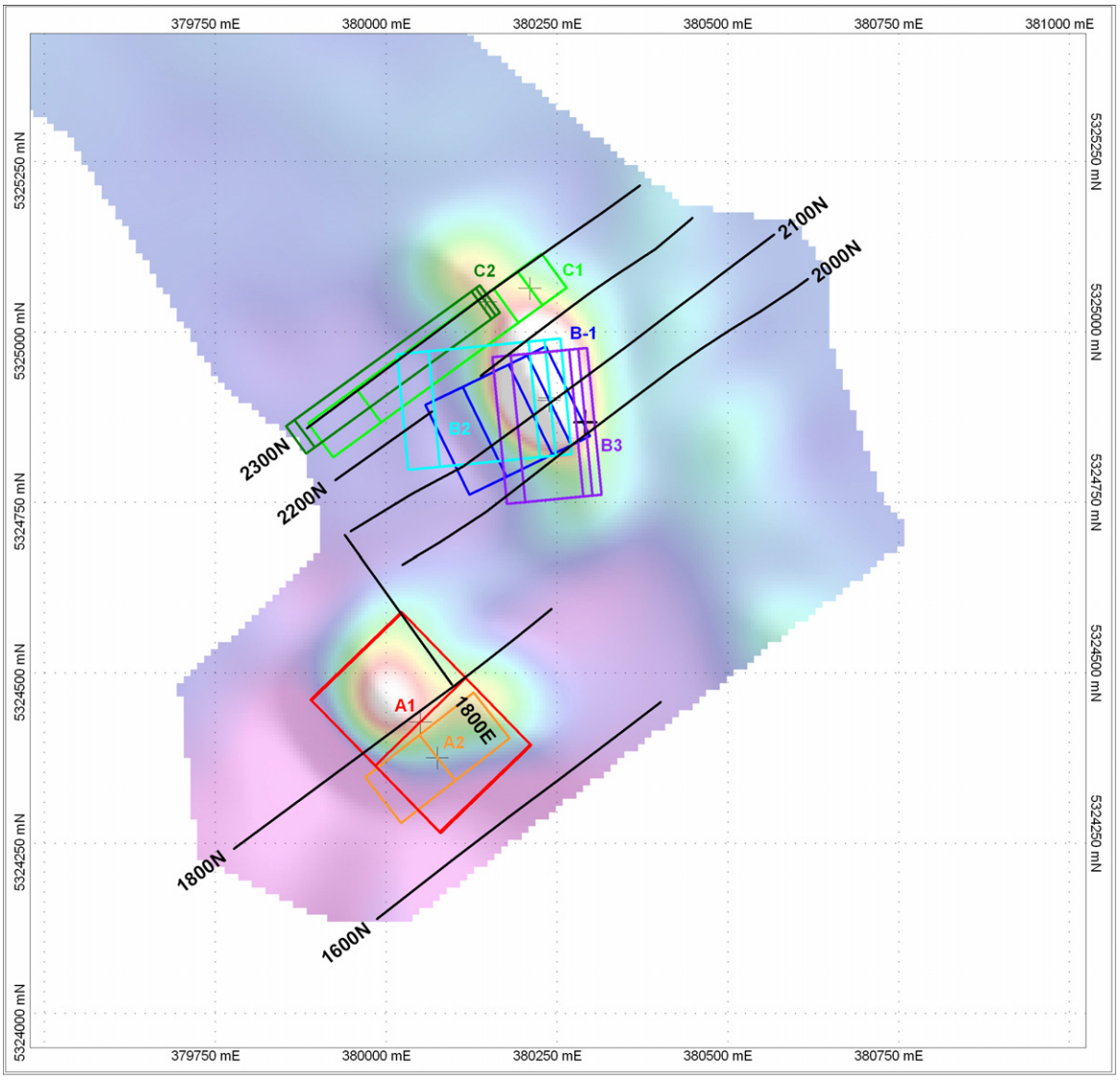

Figure 19: Plan view of modelled ground magnetic data and final models

Table 5. Model parameters for revised SGC magnetic models

Model	Model A-1	Model A-2	Model B-1	Model B-2	Model B-3	Model C-1	Model C-2
Centre Easting	380040	380070	380240	380240	380290	380210	380145
Centre Northing	5324430	5324375	5324900	5324900	5324870	5325060	5325043
Depth	60m	60m	40m	35m	75m	20m	5m
Strike Length	275m	85m	150m	170m	220m	60m	50m
Width	180m	200m	60m	50m	30m	90m	15m
Depth Extent	20m	20m	N/C	N/C	N/C	N/C	N/C
Strike	315°	320°	334°	355°	355°	324°	324°
Dip	0°	0°	72° SW	50° SW	60° SW	50° SW	50° SW
Plunge	10° NW	-	-	-	-	-	-
Mag Susc (SI)	0.14	0.34	0.16	0.21	0.24	0.024	0.045

5.3.1 Body A - Lines 1600N, 1800N and 1800E

This anomaly is not well defined by the ground magnetic data, and gridding of the anomalies on 1800N and 1800E produce an apparent anomaly peak to the north and west of these lines respectively. Thus the models generated are based on data at the flanks of the anomaly and are considered tenuous. Furthermore, there is a marked difference in the profile of line 1600N and the corresponding regional airborne magnetic data in this area. The apparent strike of body A appears to be roughly north-south in the airborne magnetic data and indicates that the source extends to the south. The relative low in the ground magnetic data from line 1600N indicates that body A does not extend as far south as this line, and also suggests a northwest–southeast strike.

The revised SGC model (Model A-1) is in agreement with Mudge (1994) in that the source is a shallow-dipping tabular body, although the SGC model is at about 60m depth (Figures 20 and 21) compared to less than 10m for the 1994 model. This variation in depth is dependent on whether the steep sided margins to the overall anomaly are considered to be part of the anomaly for body A or due to shallower surficial magnetic sources. A shallower magnetite source may explain the shallow dipole-dipole and gradient array IP anomalies in this area. Mudge (1994) also included a smaller slab offset to the west along a possible east-west fault (parallel to F1), but this second model was not required in the revised modelling in order to obtain a good fit.

An alternative model for body A (Model A-2; see Figure 19) assumes that the anomalies on 1800N and 1800E are unrelated. This model lies south of line 1800N and is also more consistent with the extent of the gradient array anomaly in this area (IP4), which only extends as far north as line 1800N.

Model A-1 should have been tested in NCT008 — there are elevated magnetic susceptibility readings (up to 0.03 SI) between 5 and 72m down hole in NCT008, that would explain the magnetic anomaly in this area. Model A-2 is so far untested by drilling.

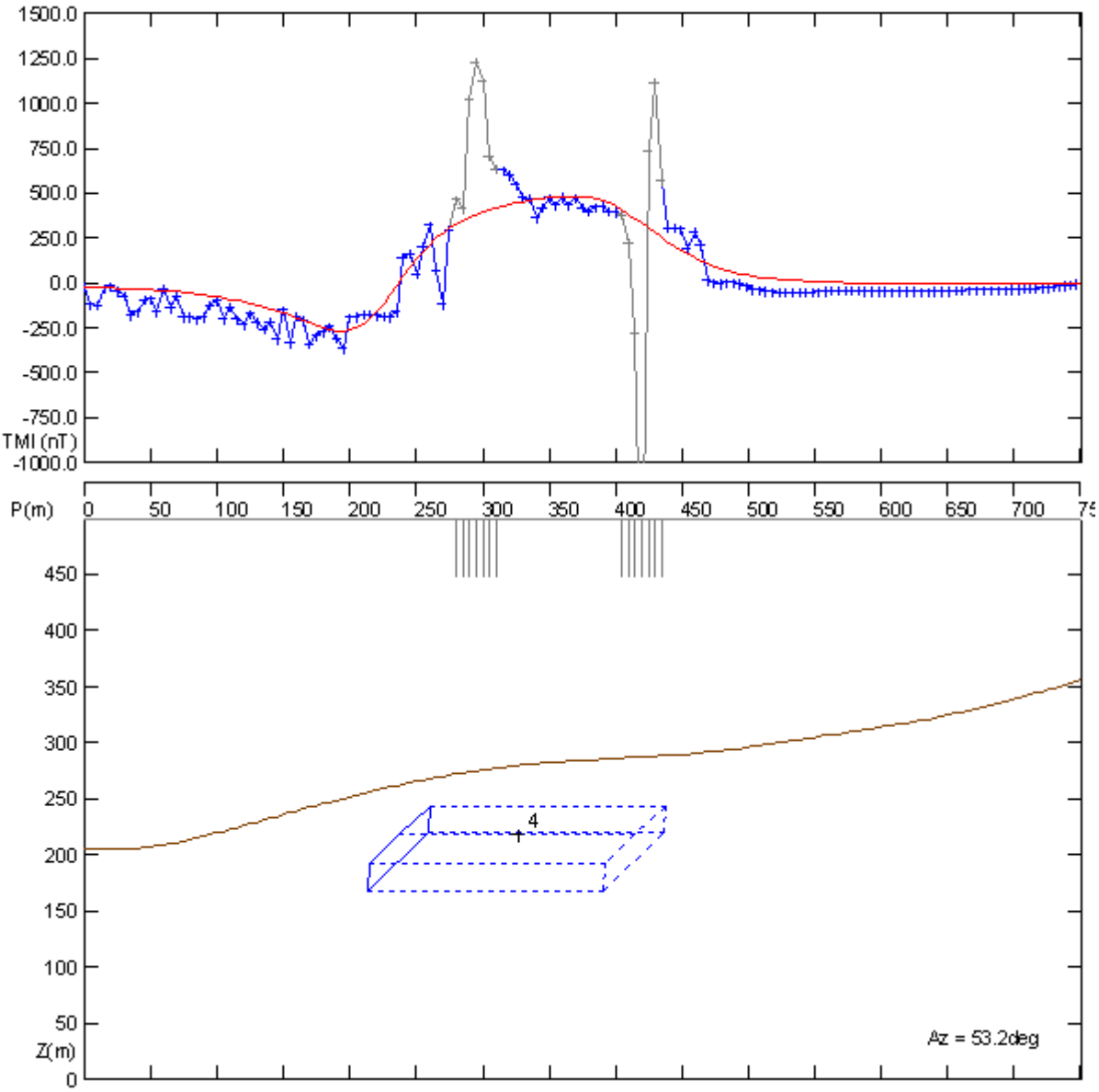

Figure 20: Magnetic Body A (Model 1) response — Line 1800N

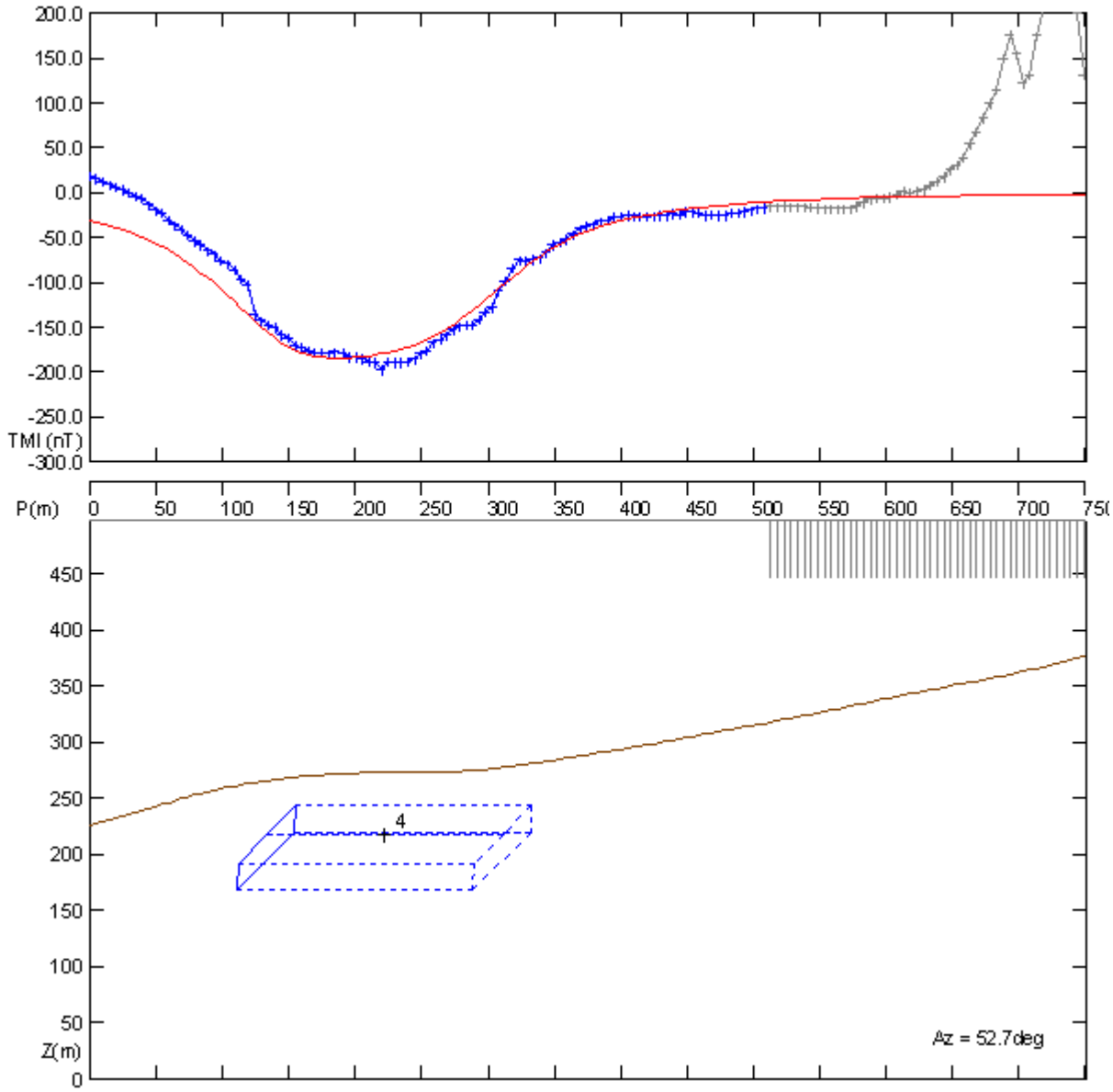

Figure 21: Magnetic Body A (Model 1) response — Line 1600N

5.3.2 Body B - Lines 2000N, 2100N and 2200N

The main anomaly associated with the andesite intrusion in the centre of the grid varies in amplitude and wavelength along strike. The peak anomaly on line 2100N has amplitude of about 1600nT, but this drops of sharply on the lines north and south to 600nT and 400nT respectively. Three models have been derived: Model 1 (Figure 22) is the best fit model over three lines (2000N, 2100N, and 2200N), Model 2 (Figure 23) was modelled solely from line 2100N, and Model 3 (Figure 24) was modelled solely from line 2000N. Overall the models show a consistent dip and physical properties. The variation in strike of the models may be reflecting some variation in orientation of the andesite intrusion along the strike, or variation in remanent magnetisation. Model 3 is deeper than the models based on the lines to the north, which suggest the depth to the top of the magnetic source increases in the vicinity of the fault — perhaps reflecting deeper weathering in this zone. Apart from Model B-1, which is more steeply dipping, the models are in general agreement dips of the magnetic units in GAR001 of 50–60° (Schmidt, 1993). It should be noted that the depth extent of these models is poorly constrained, especially when

considering that the magnetic susceptibility (and therefore influence on the anomaly shape) is decreasing with depth (Schmidt, 1993).

One of the models for Body B in Mudge (1994) is a complex trapezoidal shape in cross section for which the author recommended drilling a hole with a westerly dip. His recommended hole was never drilled. However, the new models confirm that the azimuth and inclination of historic drilling in the area was suitable for intersecting these targets. These models have been tested by GAR001, GAR002 and GAR012. The first two holes are close to the southern extent of the models. GAR001 should have intersected Model 1, whereas GAR002 narrowly misses Model 3.

The best Cu/Au intersections in these holes are approximately 30–40m shallower than the intersection with these models (Figure 25). However, the down-hole susceptibility data for GAR001 show three main anomalous intervals at around 190–200m, 230–270m and 300–320m. The central interval, which is coincident with the intersection with the magnetic Model B-1, displays the largest magnetic susceptibility (contradictory to Schmidt, 2003 — up to 0.15 SI, compared to less than 0.025 SI for the shallower interval). Therefore, although there appears to be some association between magnetite and Cu/Au mineralisation, the relationship is not linear, and the best Cu/Au concentrations may not necessarily lie within the most magnetic rocks.

GAR012 should have intersected Model B-2 at depth, but the depth extent of the models is poorly constrained, and this hole may have undershot any potential Cu/Au mineralisation associated with the intrusive body. The shallow holes in the area (GAR008, GAR009, and GAR010) do not test the magnetic body.

The existing drilling has not tested the centre of the Body 2-B models, and it is possible that the best Cu/Au intersections in GAR001 and GAR002 only represent the margin of the mineralisation.

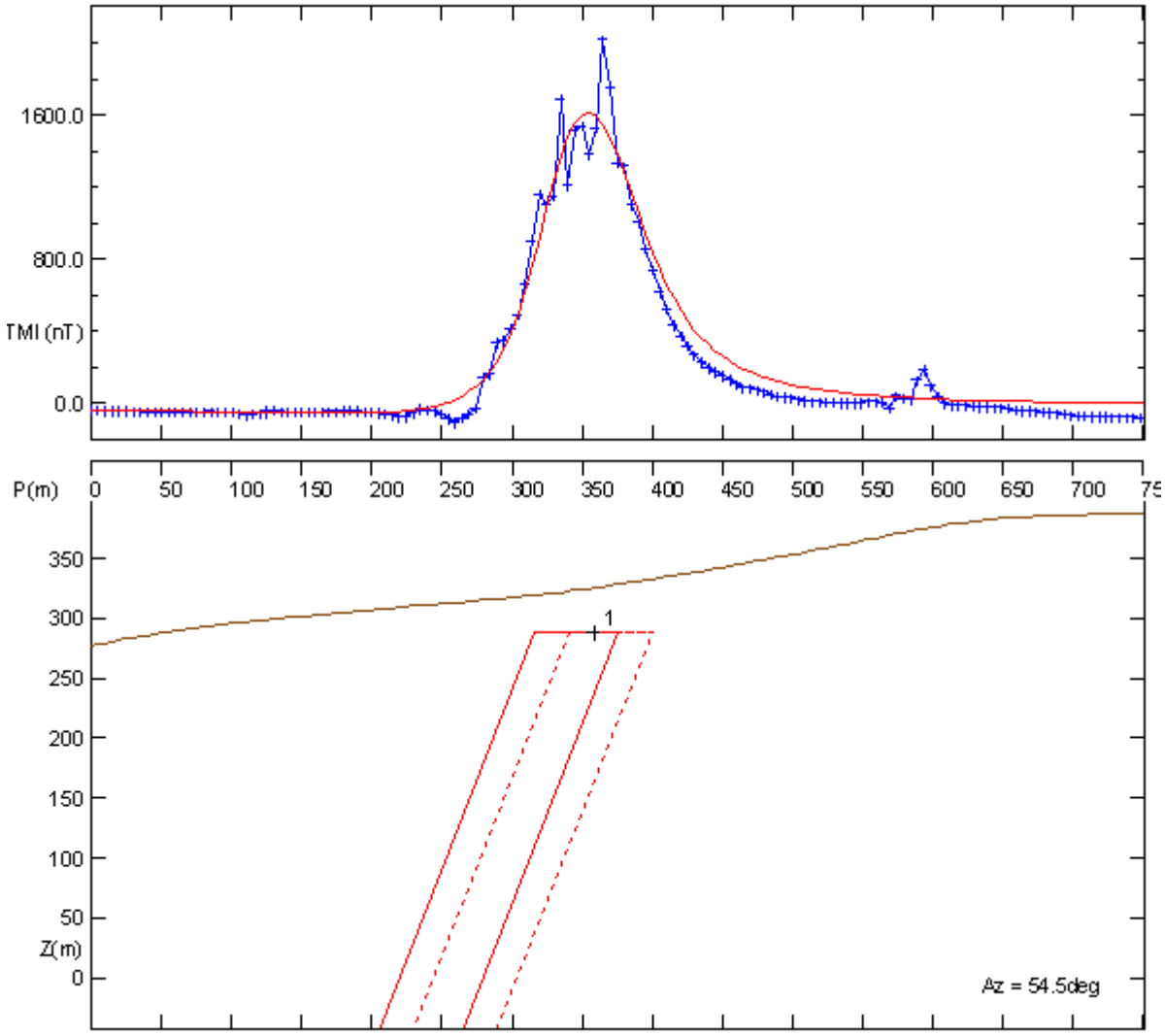

Figure 22: Magnetic Body B (Model 1) response — Line 2100N

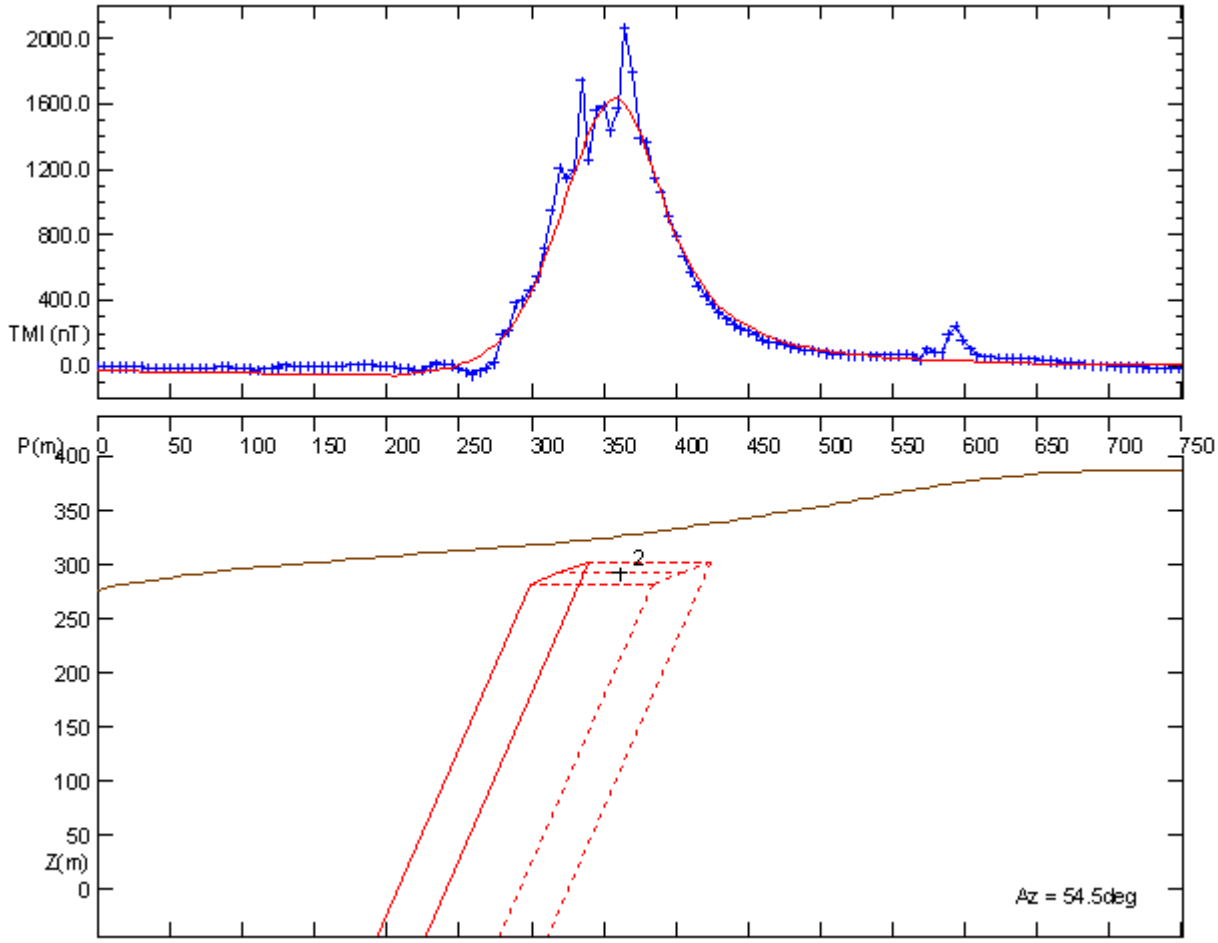

Figure 23: Magnetic Body B (Model 2) response — Line 2100N

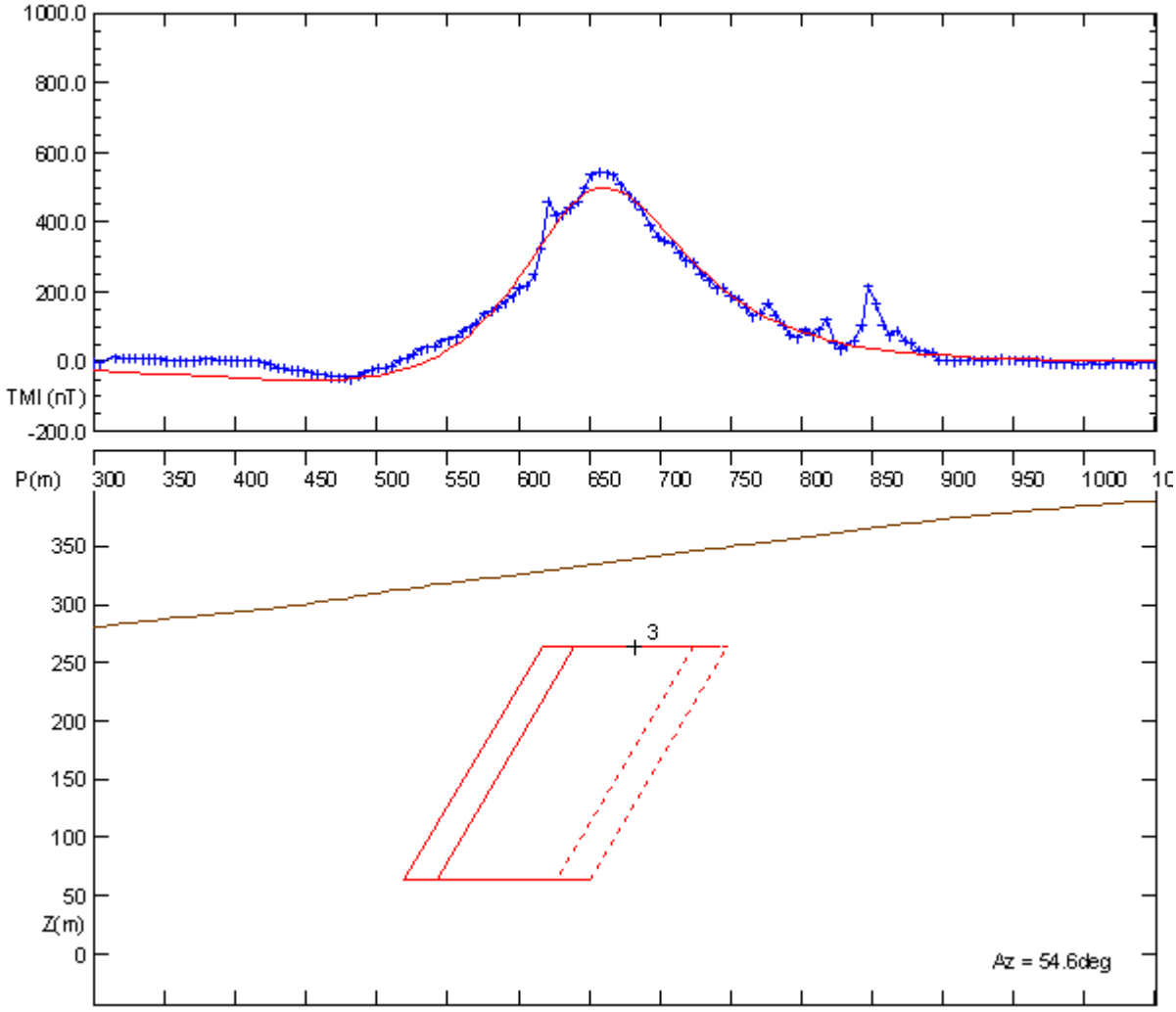

Figure 24: Magnetic Body B (Model 3) response — Line 2000N

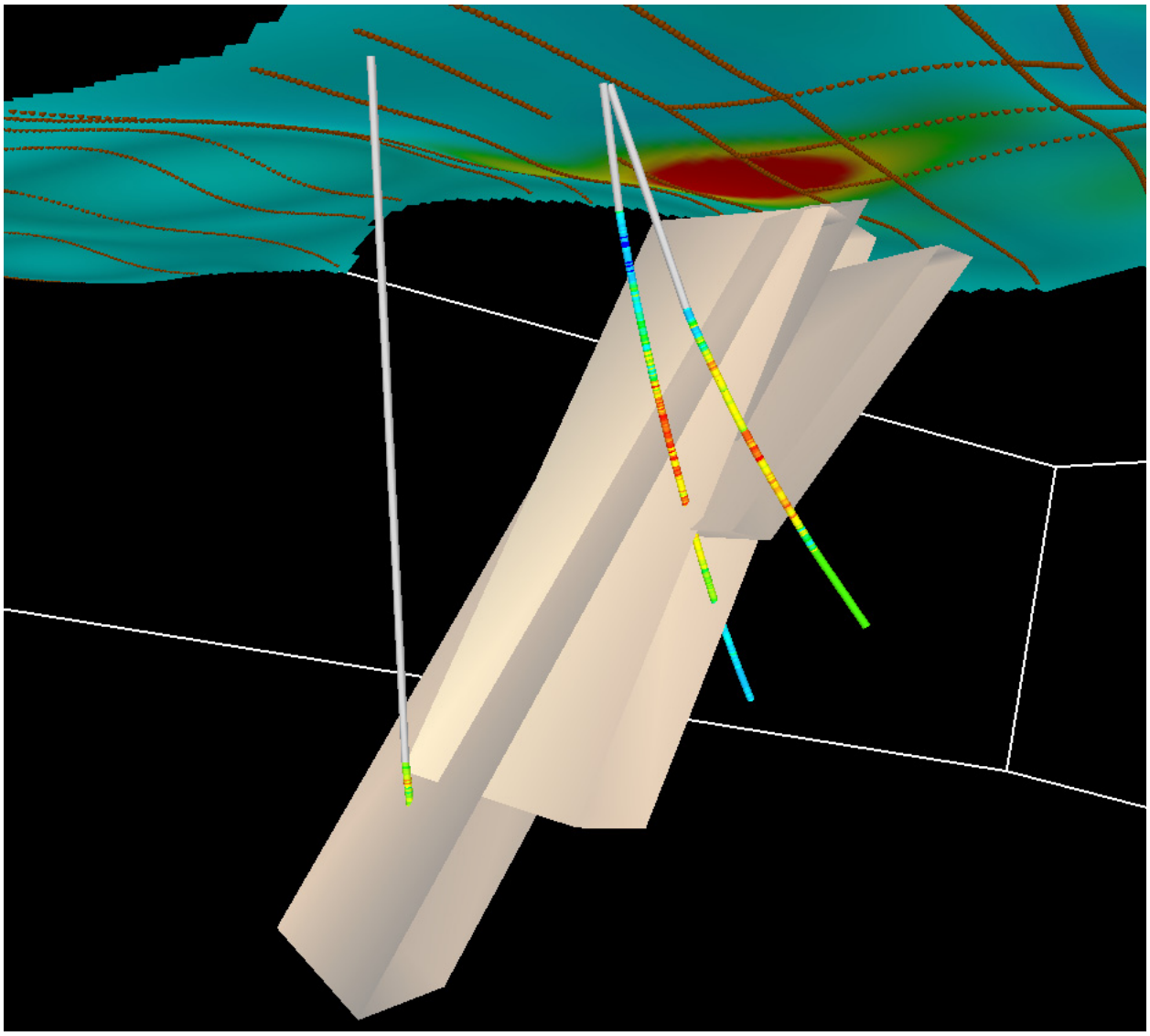

Figure 25: 3D view of GAR001, GAR002 and GAR12 coloured by Cu assay relative to the Body B models

5.3.3 Body C - Line 2300N

The anomaly on 2300N (Figure 26) is the cleanest of all the profiles to model, and looks to be the response of a shallow northerly extension to the main magnetic andesite unit (magnetic Body C), although its magnetic susceptibility is an order of magnitude lower than the Body B models to the south. These models have been tested by GAR003, the best Cu/Au assays in which correlate with the footwall contact of the main Body C model (Figure 27).

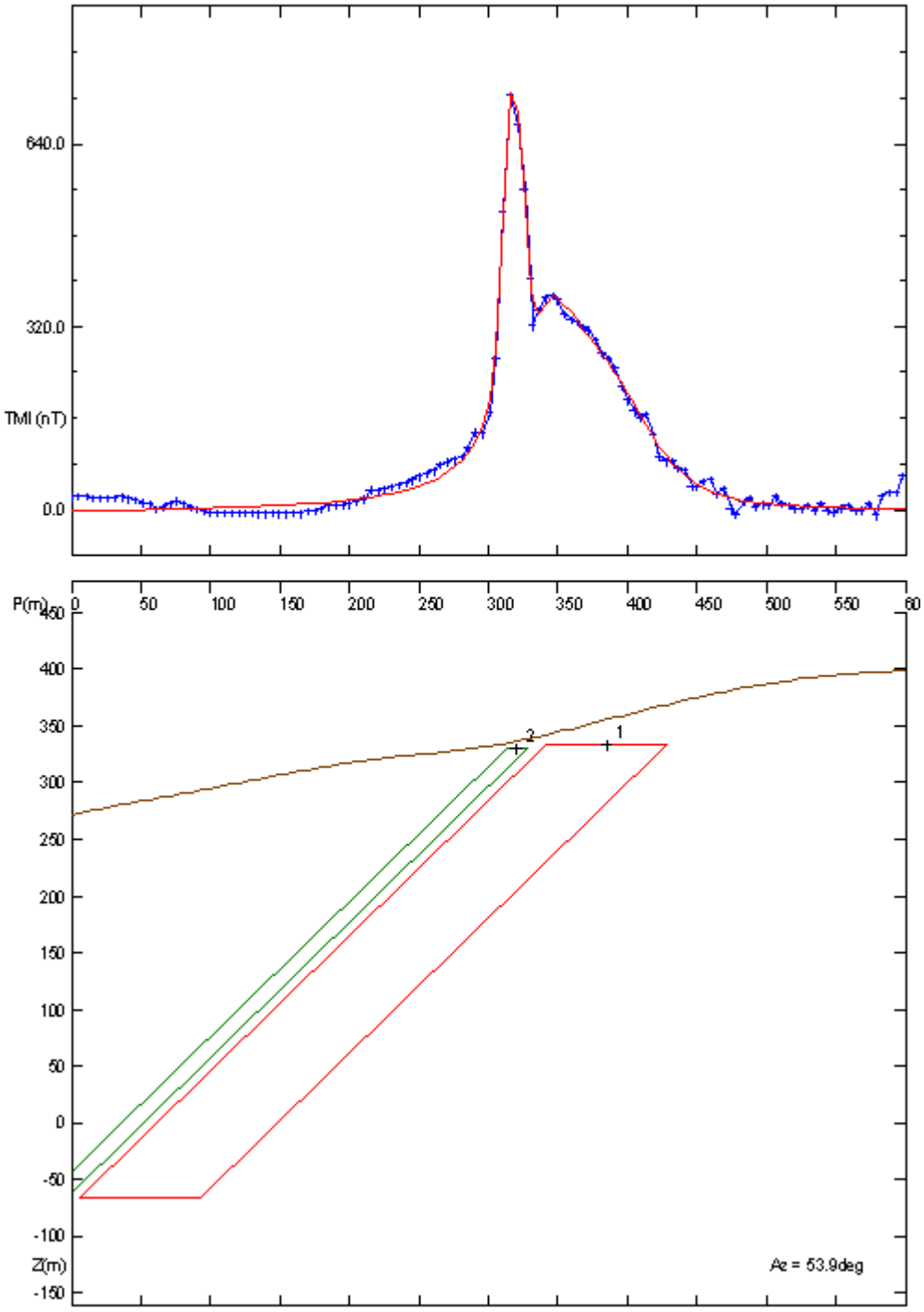

Figure 26: Magnetic Body C response (Models 1 and 2) — Line 2300N

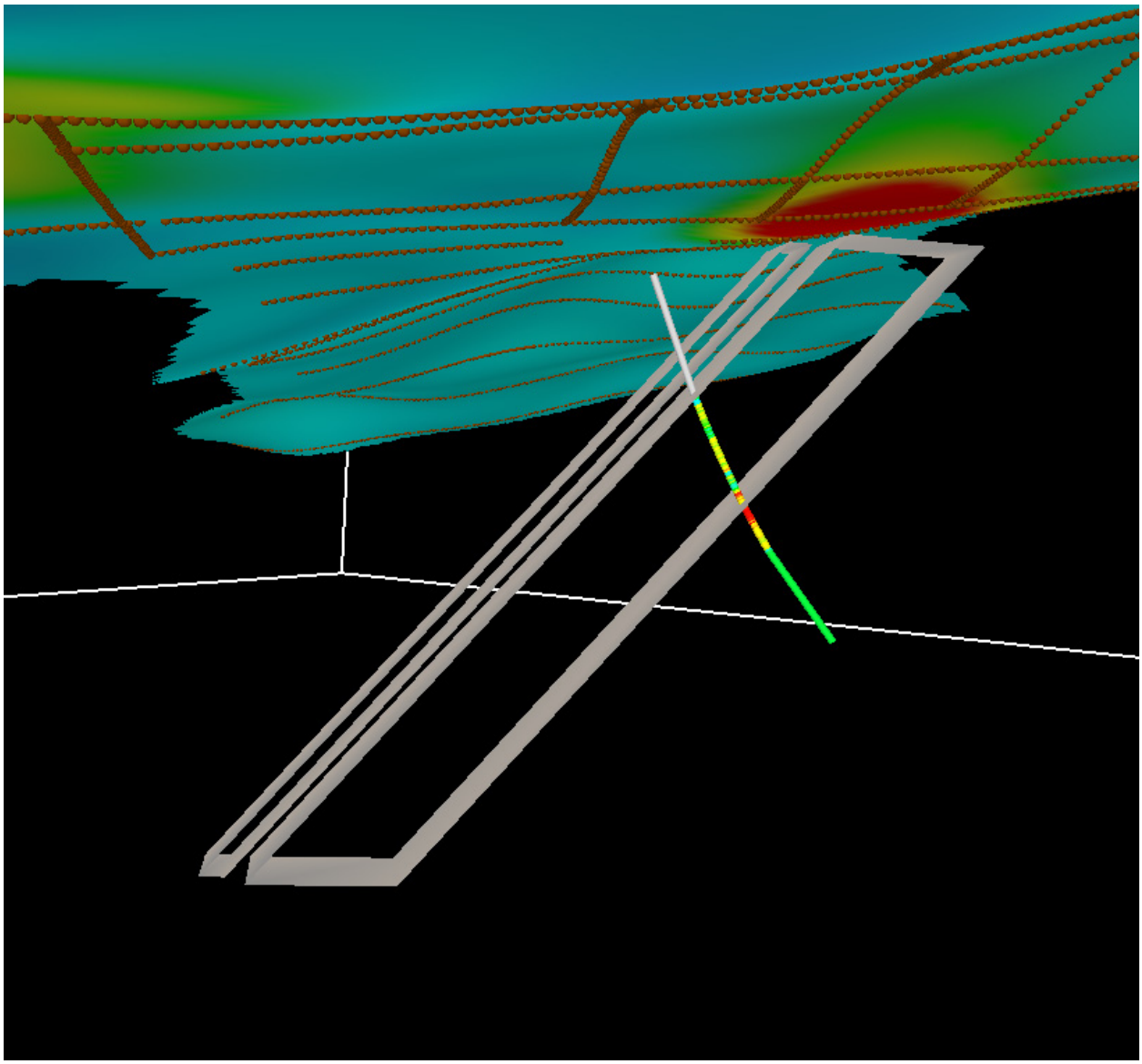

Figure 27: 3D view of GAR003, coloured by Cu assay, relative to the Body C models

5.4 Discussion

Overall the three datasets suggest that there are lithological differences between the andesitic/basaltic units mapped through the central part of the prospect, varying from moderately magnetic and chargeable between 2000N and 2250N and around 1800N, weakly magnetic and chargeable between 2250N and 2400N, to non-magnetic to the north of 2400N. The magnetic and dipole-dipole IP inversion models for the andesitic/basaltic unit to the south of the main fault F1 (Magnetic Body A) show a very different geometry to those north of F1 (Magnetic Bodies B and C). Further geological mapping and geophysical work is required to determine the structural and lithological relationships between these units.

The lack of coincident magnetic response for the gradient and dipole-dipole IP anomalies to the north of 2400N is interesting, as this discounts magnetite as the primary source of the IP anomalies in this area. More-detailed geological mapping needs to be carried out to eliminate graphitic shale as a possible source for these anomalies. The correlation between the IP anomalies in these areas and mapped volcanic units is encouraging.

6.0 CONCLUSIONS AND RECOMMENDATIONS

6.1 Conclusions

- Mudge (1994) recommended that the ground magnetic data be correctly located and elevations added to allow accurate 3D modelling. The first two of these recommendations have been carried out as part of this review. Grids of the ground magnetic data confirm that the mapped andesite units either side of the main southwest-northeast fault (F1) are moderately magnetic, but similar mapped units to the north of 2400N are not. There are discrepancies between the ground and regional airborne magnetic data reduce the confidence in the former, particularly for line 1600N, which suggests that Body A does not extend as far south as this line. Overall, there are concerns about the quality of the 1993 ground magnetic data, and this combined with variable and in some cases poor data density, means this dataset has limited use for structural and lithological interpretation.
- Some simple 3D modelling performed on the located data shows consistent moderate westerly dips for the magnetic units in the centre of the survey grid (Bodies B and C). The revised magnetic modelling confirm that the historic drilling orientation in this area was appropriate for targeting potential mineralisation associated with these magnetic units. However, the existing drilling has only tested the margins of the magnetic models, and therefore the Cu/Au intersections in GAR001 and GAR002 may not be representative of the main part of the mineralised system.
- Magnetic modelling of the anomaly in the south (Body A) is considered tenuous, but is consistent with the modelling from Mudge (2004), which suggests a flat-lying tabular magnetic body in this area. The revised model is about 50–60m deeper than that of the original model from Mudge (2004), but the latter correlates better with the gradient and dipole-dipole array IP anomalies. The geometry of this magnetic body is very different from Body B to the northeast. NCT008 may have tested the northern limit of the magnetic source, but an alternative model suggests that the source has not yet been tested by drilling to date.
- There are numerous dipole-dipole IP anomalies in the project area that have not been tested with drilling, and based on ground and airborne magnetic data, may not be sourced by magnetite. Furthermore, most of these are within or close to favourable lithologies (felsic volcanic/volcaniclastic and/or andesite/basalt geology).

  Dipole-dipole Model 1A on line 1800N is the most interesting feature in the southwestern part of the prospect. It is a strongly chargeable, shallow-dipping feature, at about 50m depth, coincident with a resistivity low. The model sits at the western margin of a volcaniclastic unit, so may be of interest in terms of possible VHMS-style mineralisation.

  In the northern part of the prospect, dipole-dipole Models 2C and 3C on lines 2800N and 3000N respectively are the most interesting features. They may represent the same chargeable body, although the gradient data shows some structural complexity between these lines. These models have some correlation with mapped dacitic lavas and volcaniclastics, and have reasonable depth extents. Models 2D, 3D and 3E correlate well with mapped andesite units, and are also of interest.

6.2 Recommendations

- Given the poor quality and reliability of the 1993 ground magnetic data and lack of any detailed airborne magnetic data, it is highly recommended that some detailed, low-level airborne magnetic data be acquired over the prospect area to aid in a detailed litho-structural interpretation.
- Mudge (1994) recommended that the gradient array coverage be extended to the southwest to close off anomaly IP4 and to the north to close off anomaly IP3. The latter was carried out in part in 1995, but the 1995 survey did join with the 1993 survey, so there is a large gap in the data coverage that could be important for confirming the relationship between anomalies IP3 and CH3. The area around IP4 is interesting, and gradient array coverage should be extended to close off this anomaly as recommended by Mudge (1994). Roberts (1995) recommended that the gradient array coverage be extended father to the north and west to test the extents anomalies CH4 and CH1. In addition to these, it may be worth extending the coverage to the southwest of CH2 to close off this anomaly also.
- Roberts (1995) recommended additional dipole-dipole array IP be conducted to improve the models for some of the anomalies, particularly 3A (model D2C in Roberts, 1995), which is on the western edge of line 3000N and has not been well resoled by the data. It is also recommended that infill lines of detailed 2D or 3D dipole-dipole data be acquired between 2600N and 3200N to better resolve the relationship between anomalies 2C, 2D, 2E, and 3C, 3D and the apparent structure that offsets the gradient array anomaly CH3 from CH4. Additional dipole-dipole lines are recommended to the southwest of anomaly 1A on line 1800N to confirm and better define this interesting dipole-dipole IP/resistivity feature.
- Given the mineralisation potential of the area, it is recommended that a more comprehensive dipole-dipole IP survey for the Garfield area be undertaken, aimed at targeting a deeper level to define potential extensions of mineralization/plunge plus any additional mineralized bodies in the general area. This survey could incorporate the Thomas Curie area to the northeast, which is poorly explored, but from airborne magnetics looks to have a similar response to the main andesite intrusion at Garfield.
- Roberts (1995) recommended drilling an easterly dipping hole collared at approximately 2050E, 3000N to target his D2B models (IP model 3C in this Report). This hole was not drilled. This anomaly, combined with the corresponding anomaly on line 2800N (Model 2C) is considered the highest priority target in this area, but the latter model suggests a steep easterly dip, and therefore a west-dipping hole may be more appropriate. More data and modelling work is recommended for this area before designing a robust drill target.

- Mudge (1994) recommended two drill holes — a west dipping hole targeting magnetic body B and the coincident gradient IP anomaly, and an east-dipping hole targeting magnetic body C and coincident gradient IP anomaly. GAR003 is close to the latter recommended hole and is considered to have adequately tested this model. The former hole was not drilled, and other drilling in the area is not considered to have adequately tested the centre of the magnetic models and coincident gradient array IP anomaly. The closest drill hole to the centre of the IP anomaly is GAR12, but this hole may have undershot the mineralisation. It is recommended that a hole be drilled on the same northing as GAR12, and easting as GAR01, to test the centre of the magnetic models for body B and coincident gradient array anomaly at a depth of approximately 140m:

  Recommended Drill Hole Parameters:

Collar East (MGA55):	380100
Collar North (MGA55):	5324900
Azimuth:	090°
Inclination:	60°
Depth:	250m (with modelled intersection from 160m)

7.0 REFERENCES

Mudge. S., 1994, Interpretation of ground magnetic and induced polarisation data, Garfield Prospect, Tasmania, E.L. 102/87; RGC Exploration, Report No TAS-GL-94/I/4

Roberts. S., 1995, A geophysical interpretation of induced polarisation surveys, October 1995, Garfield, Tasmania; RGC Exploration Report

Schmidt. P. W., 1993, Report on magnetic properties of drill core samples from the Garfield Project, Tasmania; RGC Exploration Report

Raw Spectral Pseudosection

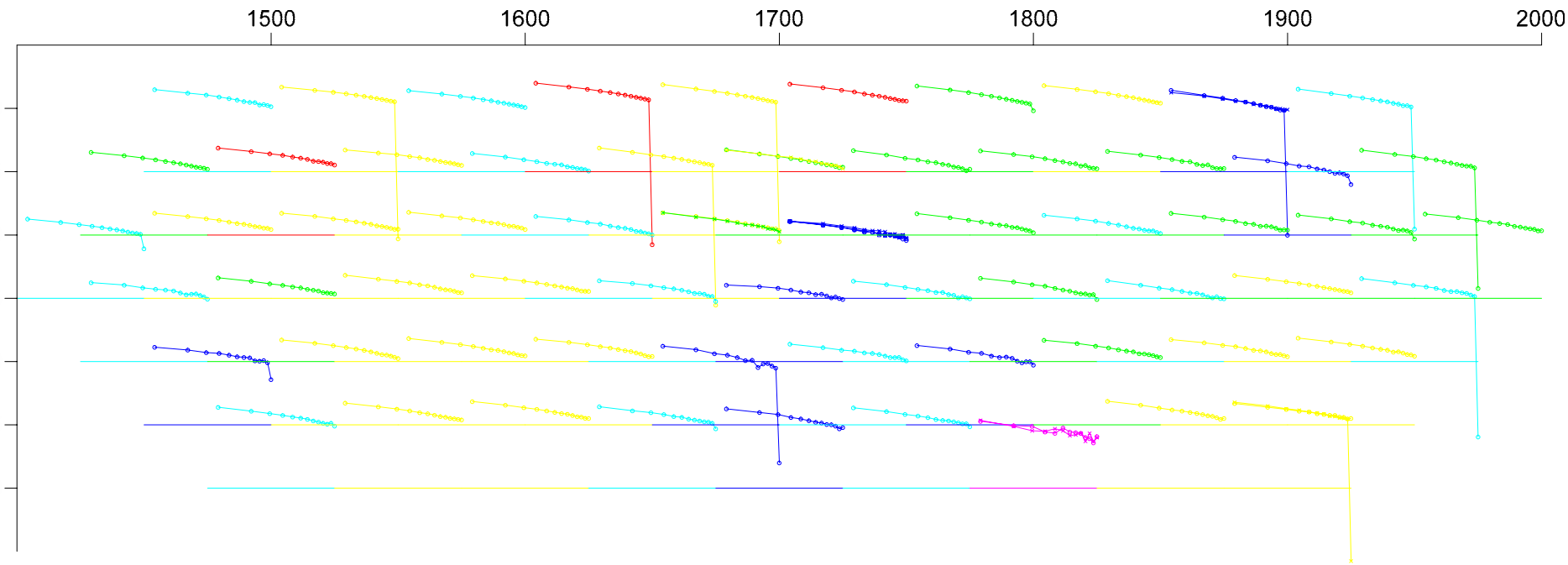

Edited and cleaned Apparent Resistivity (Ohm.m)

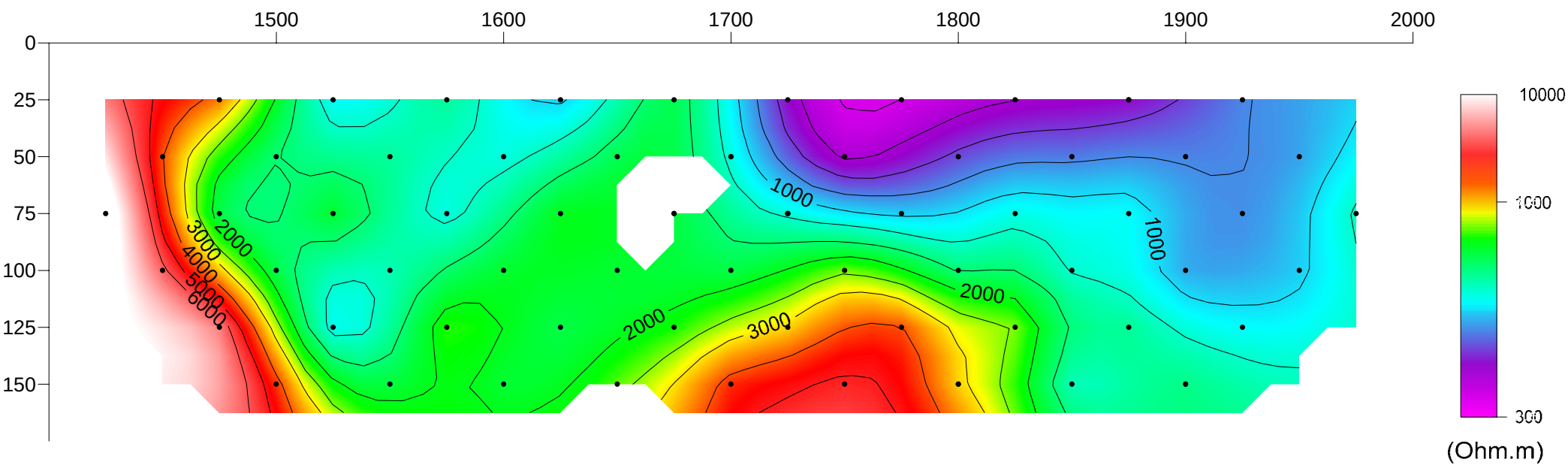

Edited and cleaned Chargeability (mV/V)

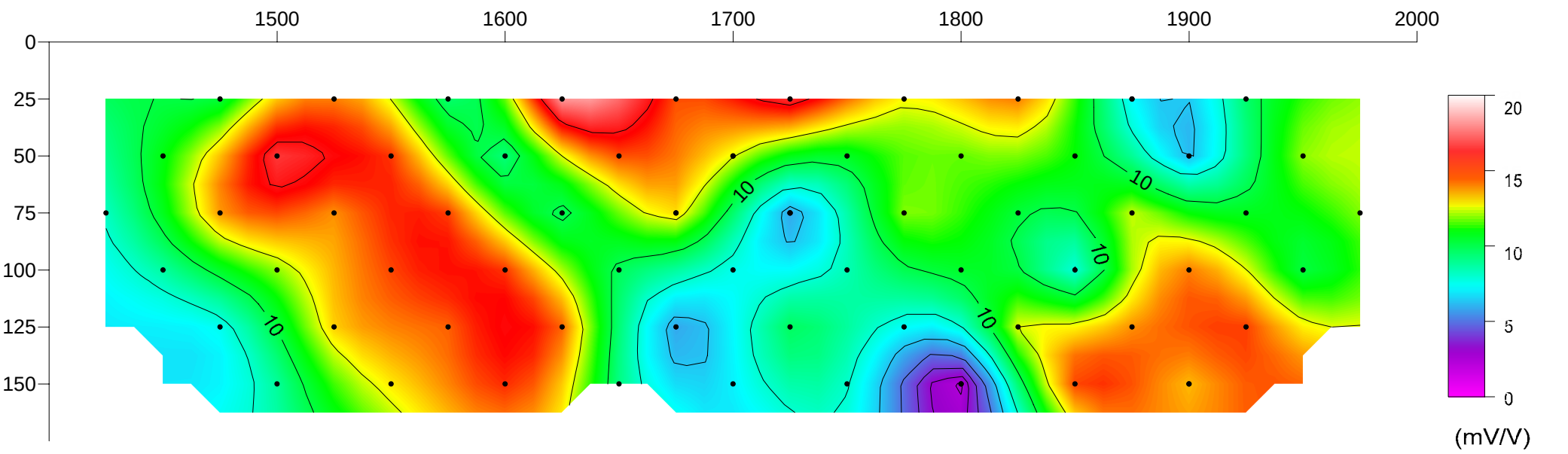

W E

Local Grid

Scale 1: 25,000

0 100 200m

Datum: GDA94
Projection: MGA55

ACQUISITION PARAMETERS

Contractor	: Geoterrex
Array	: Dipole-Dipole
Receiver	: Zonge DGP-16
Transmitter	: Huntec (7.5 kW)
Transmitter Frequency	: 0.125 Hz (2 Second cycle)
Receiver Dipole Size	: 50 m
Transmitter Dipole Size	: 50m
Transmitter Current	: 0.9-1.2 A
Date	: December 1993

DISPLAY PARAMETERS

Resistivity Contour Intervals	: 10 Levels per Decade
Chargeability Contour Intervals	: 1 mV/V

CORONA GOLD

SOUTHERN GEOSCIENCE CONSULTANTS

CORONA GOLD LTD
GARFIELD PROJECT

DIPOLE-DIPOLE
TIME-DOMAIN INDUCED POLARISATION SURVEY
Composite Pseudosections
LINE 1800N

Date: 21 February 2011	Geophysicist: KAB
Garfield_Line_1800N.pdf	

Raw Spectral Pseudosection

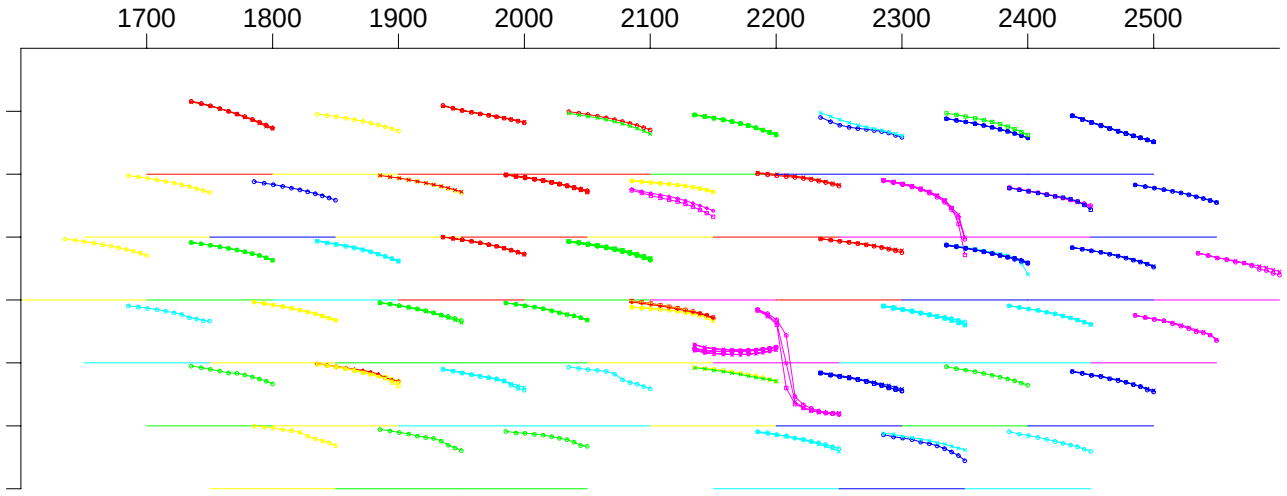

Scale 1: 60,000

0 100 200 300m

W E

Local Grid

Edited, Cleaned and Averaged Spectral Pseudosection

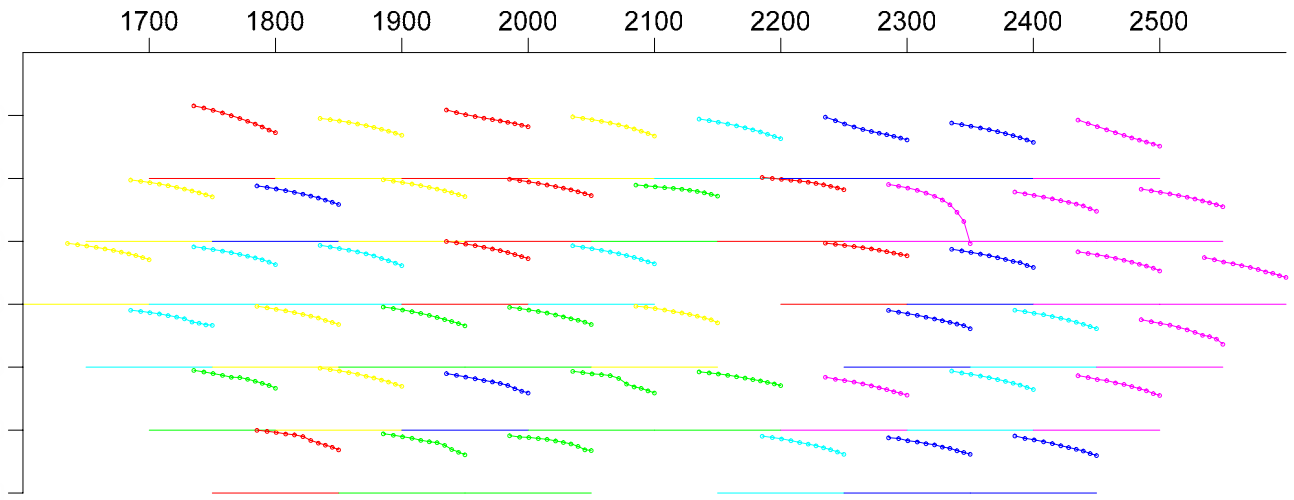

Edited and cleaned Apparent Resistivity (Ohm.m)

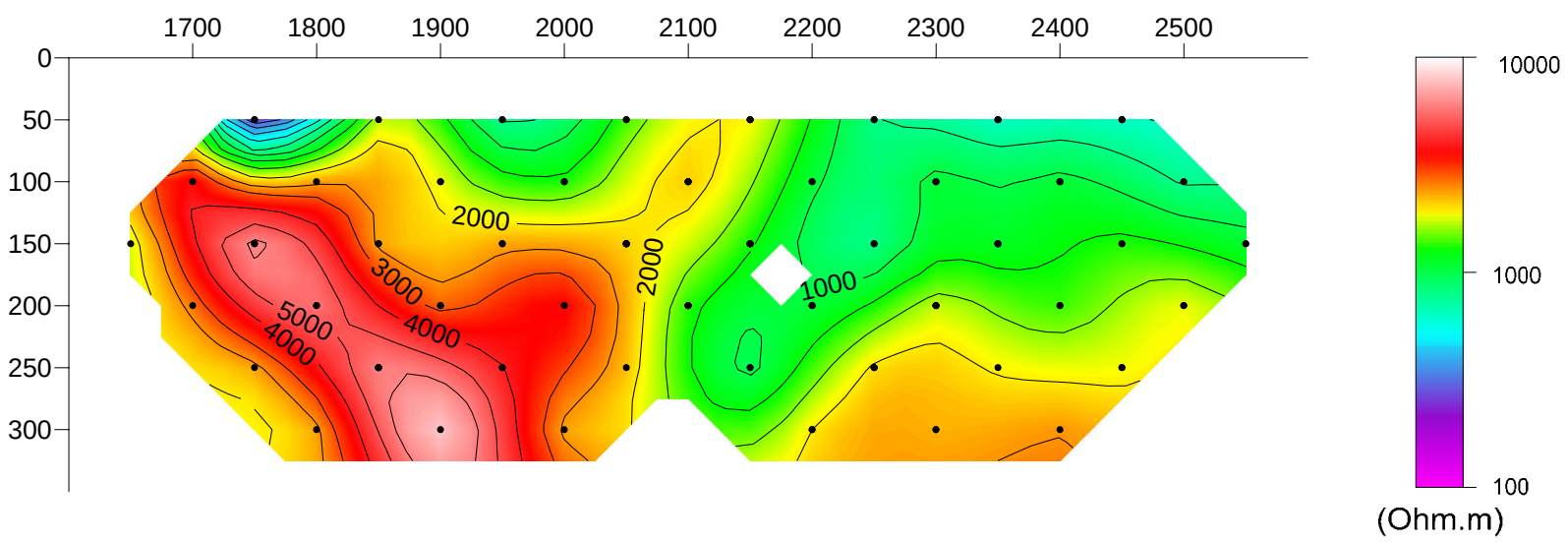

(Ohm.m)

Edited and cleaned Chargeability (mV/V)

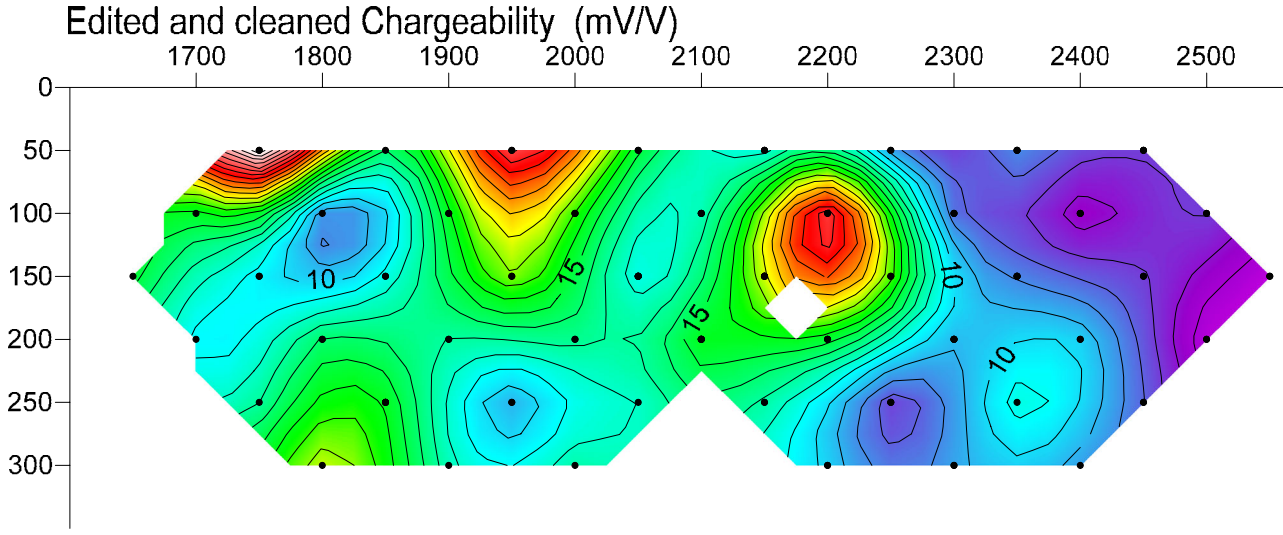

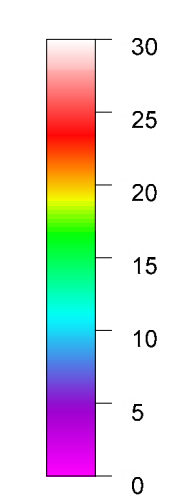

(mV/V)

ACQUISITION PARAMETERS

Contractor	: Quadrant Geophysics
Array	: Dipole-Dipole
Receiver	: IPR12
Transmitter	: Zonge GGT-2.5 (2.5 kW)
Transmitter Frequency	: 0.125 Hz (2 Second cycle)
Receiver Dipole Size	: 100 m
Transmitter Dipole Size	: 100m
Transmitter Current	: Unknown
Date	: October 1995

DISPLAY PARAMETERS

Resistivity Contour Intervals	: 10 Levels per Decade
Chargeability Contour Intervals	: 1 mV/V

CORONA GOLD

SOUTHERN GEOSCIENCE CONSULTANTS

CORONA GOLD LTD
GARFIELD PROJECT

DIPOLE-DIPOLE
TIME-DOMAIN INDUCED POLARISATION SURVEY
Composite Pseudosections
LINE 2800N

Date: 18 February 2011	Geophysicist: KAB
Garfield_Line_2800N.pdf	

Raw Spectral Pseudosection

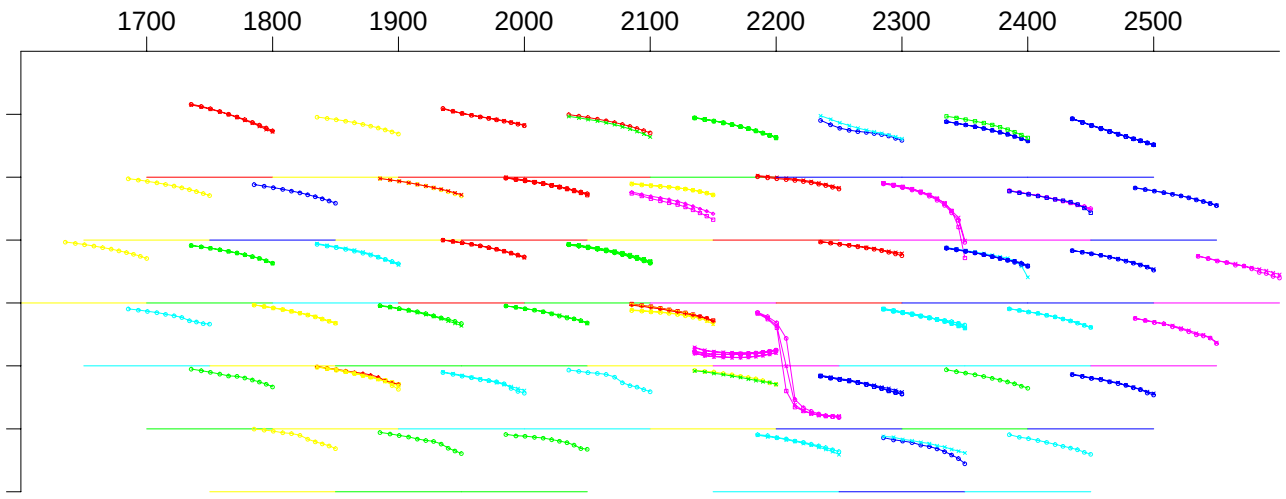

Scale 1: 60,000

0 100 200 300m

W E

Local Grid

Edited, Cleaned and Averaged Spectral Pseudosection

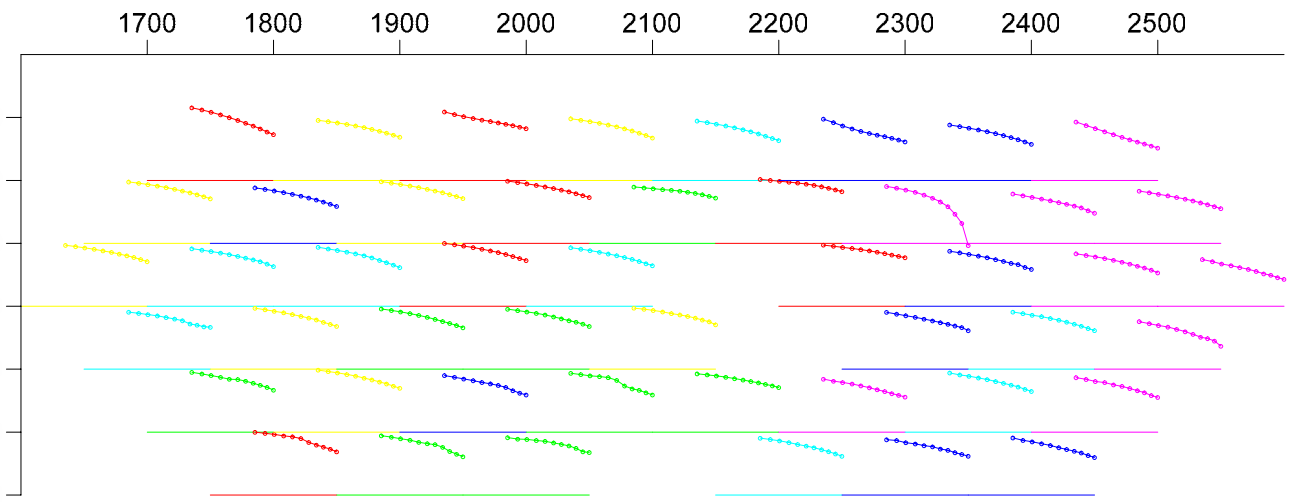

Edited and cleaned Apparent Resistivity (Ohm.m)

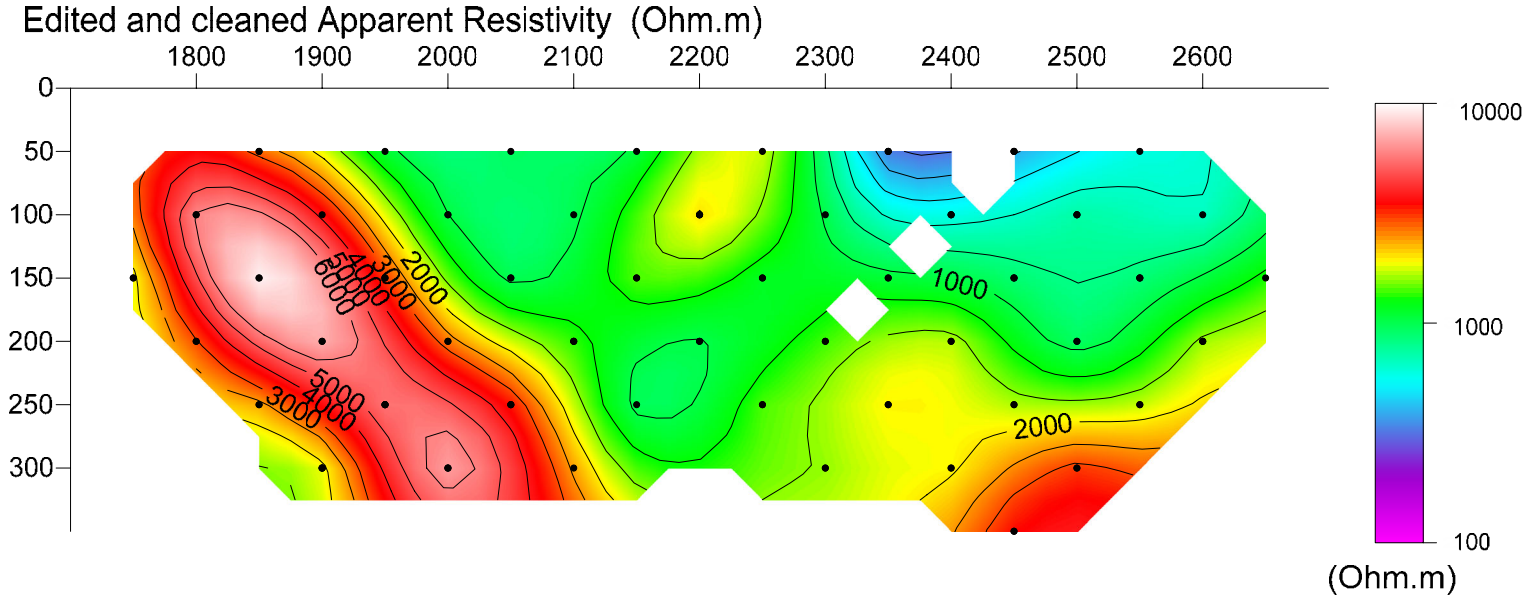

Edited and cleaned Chargeability (mV/V)

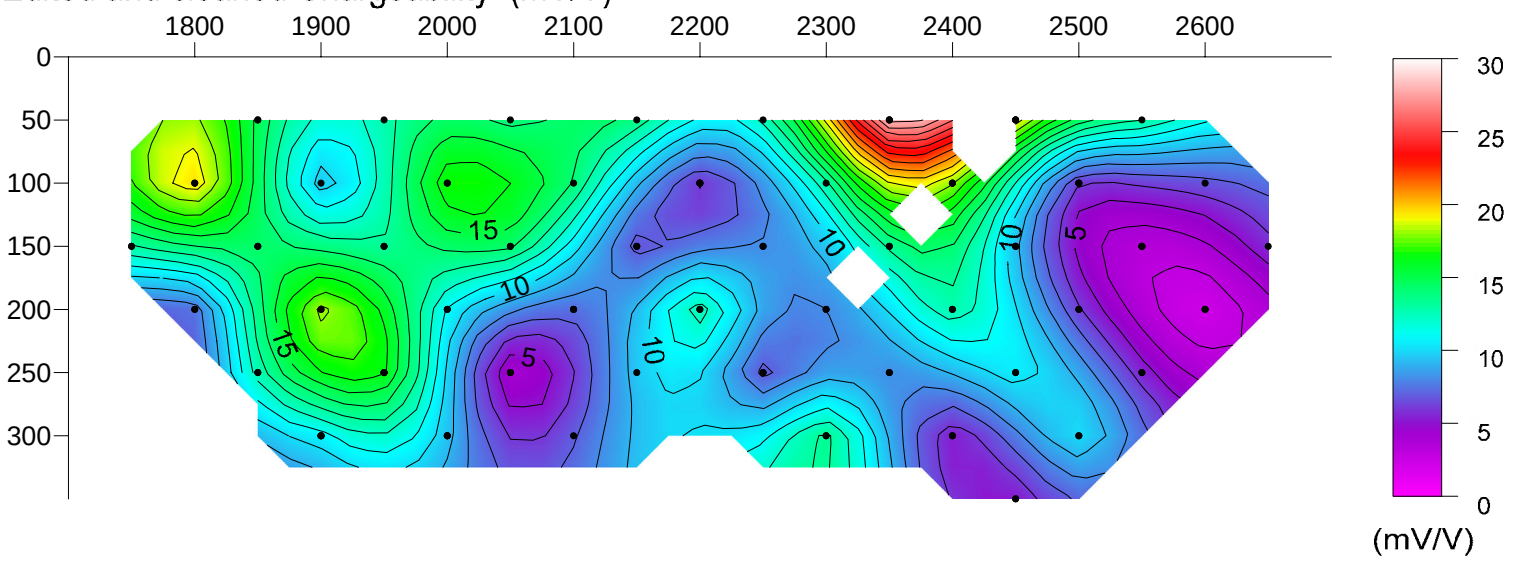

ACQUISITION PARAMETERS

Contractor	: Quadrant Geophysics
Array	: Dipole-Dipole
Receiver	: IPR12
Transmitter	: Zonge GGT-2.5 (2.5 kW)
Transmitter Frequency	: 0.125 Hz (2 Second cycle)
Receiver Dipole Size	: 100 m
Transmitter Dipole Size	: 100m
Transmitter Current	: Unknown
Date	: October 1995

DISPLAY PARAMETERS

Resistivity Contour Intervals	: 10 Levels per Decade
Chargeability Contour Intervals	: 1 mV/V

CORONA GOLD

SOUTHERN GEOSCIENCE CONSULTANTS

CORONA GOLD LTD
GARFIELD PROJECT

DIPOLE-DIPOLE
TIME-DOMAIN INDUCED POLARISATION SURVEY
Composite Pseudosections
LINE 3000N

Date: 21 February 2011	Geophysicist: KAB

Garfield_Line_2800N.pdf

APPENDIX 1

2D Dipole-Dipole Psuedesection Compilations

APPENDIX 2

2D Dipole-Dipole Inversion Parameters

Inversion settings

Initial damping factor (0.01 to 1.00)

0.1000

Minimum damping factor (0.001 to 0.75)

0.0050

Line search option (0=Never, 1=Sometimes, 2=Always)

2

Convergence limit for relative change in RMS error in percent (0.1 to 20)

5.0000

Minimum change in RMS error for line search in percent (0.5 to 100)

0.5000

Number of iterations (1 to 30)

7

Vertical to horizontal flatness filter ratio (0.25 to 4.0)

1.0000

Model for increase in thickness of layers(0=default 10, 1=default 25, 2=user defined)

2

Number of nodes between adjacent electrodes (2 or 4)

2

Flatness filter type, Include smoothing of model resistivity (0=model changes only,1=directly on model)

1

Reduce number of topographical datum points? (0=No,1=Yes. Recommend leave at 0)

0

Carry out topography modeling? (0=No,1=Yes)

1

Type of topography trend removal (0=Average,1=Least-squares,2=End to end)

0

Type of Jacobian matrix calculation (0=Quasi-Newton, 1=Gauss-Newton, 2=Mixed)

1

Increase of damping factor with depth (1.0 to 2.0)

1.1000

Type of topographical modeling (0=None, 1=No longer supported so do not use, 2=uniform distorted FEM, 3=underwater, 4=damped FEM, 5=FEM with inverse Swartz-Christoffel)

4

Robust data constrain? (0=No, 1=Yes)

1

Cutoff factor for data constrain (0.0001 to 0.1))

0.0500

Robust model constrain? (0=No, 1=Yes)

0

Cutoff factor for model constrain (0.0001 to 1.0)

0.0050

Allow number of model parameters to exceed datum points? (0=No, 1=Yes)

1

Use extended model? (0=No, 1=Yes)

1

Reduce effect of side blocks? (0=No, 1=Slight, 2=Severe, 3=Very Severe)

0

Type of mesh (0=Normal,1=Fine,2=Finest)

0

Optimise damping factor? (0=No, 1=Yes)

1

Time-lapse inversion constrain (0=None,1=Least-squares,2=Smooth,3=Robust)

0

Type of time-lapse inversion method (0=Simultaneous,1=Sequential)

0

Thickness of first layer (0.25 to 1.0)

0.4000

Factor to increase thickness layer with depth (1.0 to 1.25)

1.1000

USE FINITE ELEMENT METHOD (YES=1,NO=0)

1

WIDTH OF BLOCKS (1=NORMAL WIDTH, 2=DOUBLE, 3=TRIPLE, 4=QUADRAPLE, 5=QUINTIPLE)

1

MAKE SURE BLOCKS HAVE THE SAME WIDTH (YES=1,NO=0)

1

RMS CONVERGENCE LIMIT (IN PERCENT)

0.050

USE LOGARITHM OF APPARENT RESISTIVITY (0=USE LOG OF APPARENT RESISTIVITY, 1=USE RESISTANCE VALUES, 2=USE APPARENT RESISTIVITY)

2

TYPE OF IP INVERSION METHOD (0=CONCURRENT,1=SEQUENTIAL)

0

PROCEED AUTOMATICALLY FOR SEQUENTIAL METHOD (1=YES,0=NO)

0

IP DAMPING FACTOR (0.01 to 1.0)

0.100

USE AUTOMATIC IP DAMPING FACTOR (YES=1,NO=0)

0

CUTOFF FACTOR FOR BOREHOLE DATA (0.0005 to 0.02)

0.00010

TYPE OF CROSS-BOREHOLE MODEL (0=normal,1=halfsize)

0

LIMIT RESISTIVITY VALUES(0=No,1=Yes)

0

Upper limit factor (10-50)

50.000

Lower limit factor (0.02 to 0.1)

0.020

Type of reference resistivity (0=average,1=first iteration)

0

Model refinement (1.0=Normal,0.5=Half-width cells)

0.50

Combined Combined Marquardt and Occam inversion (0=Not used,1=used)

0

Type of optimisation method (0=Gauss-Newton,2=Incomplete GN)

0

Convergence limit for Incomplete Gauss-Newton method (0.005 to 0.05)

0.005

Use data compression with Incomplete Gauss-Newton (0=No,1=Yes)

0

Use reference model in inversion (0=No,1=Yes)

0

Damping factor for reference model (0.0 to 0.3)

0.01000

Use fast method to calculate Jacobian matrix. (0=No,1=Yes)

1

Use higher damping for first layer? (0=No,1=Yes)

1

Extra damping factor for first layer (1.0 to 100.0)

5.00000

Type of finite-element method (0=Triangular,1=Trapezoidal elements)

1

Factor to increase model depth range (1.0 to 5.0)

1.100

Reduce model variations near borehole (0=No, 1=Yes)

0

Factor to control the degree variations near the boreholes are reduced (2 to 100)

5.0

Factor to control variation of borehole damping factor with distance (0.5 to 5.0)

1.0

Floating electrodes survey inversion method (0=use fixed water layer, 1=Incorporate water layer into the model)

1

Resistivity variation within water layer (0=allow resistivity to vary freely,1=minimise variation)

1

Use sparse inversion method for very long survey lines (0=No, 1=Yes)

0

Optimize Jacobian matrix calculation (0=No, 1=Yes)

0

Automatically switch electrodes for negative geometric factor (0=No, 1=Yes)

1

Force resistance value to be consistant with the geometric factor (0=No, 1=Yes)

0

Shift the electrodes to round up positions of electrodes (0=No, 1=Yes)

0

Use difference of measurements in time-lapse inversion (0=No,1=Yes)

0

Use active constraint balancing (0=No,1=Yes)

0

Type of active constraints (0=Normal,1=Reverse)

0

Lower damping factor limit for active constraints

0.4000

Upper damping factor limit for active constraints

2.5000

Water resistivity variation damping factor

8.0000